Tectonophysics 765 (2019) 102–128

Contents lists available at ScienceDirect

Tectonophysics

journal homepage: www.elsevier.com/locate/tecto

Tectonics of the northern Canadian Cordillera imaged using modern magnetotelluric analysis

Banafsheh Habibian Dehkordi[a,*], Ian J. Ferguson[b], Alan G. Jones[c], Juanjo Ledo[d], Grant Wennberg[b,1]

[a] Institute of Geophysics, University of Tehran, Tehran, Iran
[b] Dept. of Geological Sciences, University of Manitoba, Winnipeg, Manitoba, Canada
[c] Complete MT Solutions, Ottawa, Ontario, Canada; Formerly Dublin Institute for Advanced Studies, Dublin, Ireland
[d] Universitat de Barcelona, Barcelona, Spain

ARTICLE INFO

Keywords:
Magnetotellurics
Northern Canadian Cordillera
Resistivity

ABSTRACT

Magnetotelluric data from LITHOPROBE SNORCLE Corridor 2 in western Canada crossing the Rocky Mountain Trench-Tintina Fault between 56° and 60°N have been analyzed using modern MT methods to provide new insights into the tectonics of the North American Cordillera and Ancestral North America. Resistivity images of the crust were obtained using two independent sets of unconstrained 2-D inversions and constrained 2-D inversions incorporating seismic constraints. Structure to the west of the Tintina Fault includes uniform, moderate, mid to lower crustal resistivity in a seismically-defined westward-tapering wedge of Ancestral North American rocks. To the east, between the Tintina Fault and the Liard line, a transfer zone in asymmetric Neoproterozoic rifting, the wedge includes a major synformal conductor that parallels seismic reflections. The large lateral changes in resistivity can be explained by transition between different blocks of asymmetric rifting. The synformal conductor is attributed to graphitic rocks from the Aida Formation of the Mesoproterozoic Muskwa Assemblage that were re-distributed in a sag basin on the lower plate margin in the Blackwater Block. Spatially-complex upper crustal resistivity in the Cordillera can be interpreted in terms of lithological variations and alteration processes. An east-dipping conductor in Stikinia is attributed to east-dipping Jurassic and relatively high conductivity beneath the Eskay rift may be explained by crustal fertilization. A conductor in the Cache Creek terrane is attributed to listwanite alteration of ultramafic bodies on the King Salmon Fault, and high conductivity in the Slide Mountain terrane within the Sylvester Allochthon to localized carbonaceous alteration. A series of conductors above North American Basement is attributed to deformation and metamorphic processes associated with Mesozoic thrust faulting. To the west of the Tintina Fault the source material for these conductors is likely from the Stikinia terrane, and to the east it is likely from the Muskwa Assemblage.

1. Introduction

The North American Cordillera is a billion-year old accretionary orogen forming a continental-scale mountain range. The development of the Cordillera began with the formation of the Laurentian margin in the Neoproterozoic era followed by continental passive margin deposition during early Palaeozoic time (e.g., Monger, 1989; Colpron and Nelson, 2009). In the middle Palaeozoic the margin became active as subduction was initiated and a convergent margin tectonic setting has continued to the present time. This convergence has resulted in the growth of the margin through the progressive addition of a large number of exotic terranes and margin rocks (e.g., Coney et al., 1980; Gabrielse et al., 1991; Monger, 1989; Colpron and Nelson, 2009).

The Canadian Cordillera was investigated in geophysics-focused studies in two transects in the Canadian national LITHOPROBE project (e.g., Cook et al., 2012). The Southern Cordilleran Transect (SCCT in Fig. 1 inset) focused on studies between 49°N and 52°N (Clowes, 1993) and the Slave-Northern Cordillera Lithospheric Evolution (SNORCLE) Transect (SNORCLE in Fig. 1 inset) included studies between 55°N and 64°N as well as studies of the Slave craton and Wopmay orogen to the east. A number of more recent large-scale geophysical investigations have been conducted in the Canadian Cordillera including studies done

* Corresponding author.
E-mail addresses: bhabibian@ut.ac.ir (B. Habibian Dehkordi), Ij.Ferguson@umanitoba.ca (I.J. Ferguson), jledo@ub.edu (J. Ledo), grant.wennberg@dvn.com (G. Wennberg).
[1] Now at Devon Energy, Calgary, Canada.

https://doi.org/10.1016/j.tecto.2019.05.012
Received 3 December 2018; Received in revised form 8 May 2019; Accepted 15 May 2019
Available online 21 May 2019

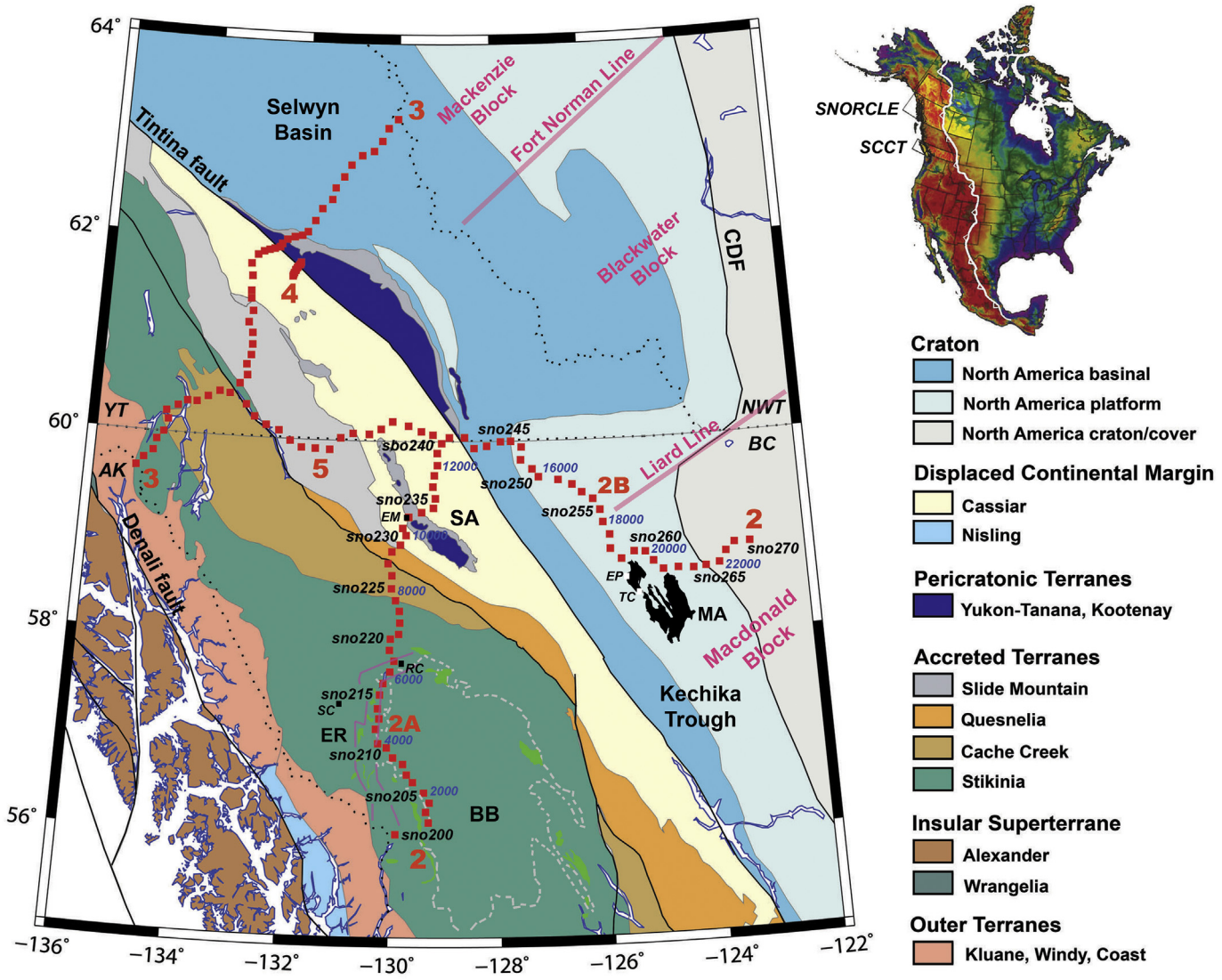

Fig. 1. Tectonic map of northwestern Canada showing locations of the LITHOPROBE SNORCLE corridors and geological features discussed in the text. MT sites are shown by red squares and black labels and selected seismic reflection vibration points (VP) are shown by blue labels. Geographic abbreviations: AK = Alaska; YT = Yukon Territory; NWT = Northwest Territories; BC = British Columbia. Geological abbreviations: MA = Muskwa Anticlinorium; SA = Sylvester Allochthon; BB = Bowser Basin; ER = Eskay Rift and CDF = Cordilleran Deformation Front. Mine or deposit abbreviations: SC = Schaft Creek porphyry Cu mine; RC = Red Chris porphyry Cu mine; EM = Erickson Au mine; EP = Eagle Creek Cu-Ag-Pb-Co-Zn property; TC = Toro Churchill Cu property. Pink lines and labels denote prominent lineaments and blocks of North American margin (Cecile et al., 1997). Light green shading near margins of the Bowser Basin show the Upper Hazleton Group (Gagnon et al., 2012). The location of additional faults is shown on subsequent figures. Inset shows the location of the Cordillera in North America and the LITHOPROBE SNORCLE and Southern Cordillera (SCCT) projects (Cook et al., 2012). White line on the inset is the Cordilleran deformation front. (For interpretation of the references to colour in this figure legend, the reader is referred to the web version of this article.)

as part of the POLARIS project (Eaton et al., 2005) and proposals are under development for synoptic geophysical imaging of the region similar to that in the United States Earthscope program (Boggs et al., 2018).

The magnetotelluric (MT) method (e.g., Vozoff, 1991; Chave and Jones, 2012) was applied as a major geophysical component of both the LITHOPROBE SCCT and SNORCLE transects to study the electrical resistivity structure of the Earth's crust and upper mantle. The MT method has many applications in lithospheric studies where it can define tectonic structures such as faults and terrane boundaries and elucidate the processes that have formed, preserved and changed the lithosphere (Ferguson et al., 2012). The distribution of enhanced conductivity can map processes associated with plate tectonics such as metamorphism of carbonaceous accretionary-wedge sediments (e.g., Boerner et al., 1996; Yang, 2011). MT can provide information on faults and shear zones (Ritter et al., 2005; Ledo et al., 2002a; Yin et al., 2014) and locally, mantle electrical resistivity is sensitive to graphite, sulphides, partial melts, fertility, and redox (e.g., Selway, 2014).

The main objectives of the SNORCLE MT studies were (1) characterization of the regional conductivity properties of the northern Cordillera, (2) imaging upper mantle features, and (3) determination of the subsurface geometry and character of the Tintina strike-slip fault zone. The goal of the present study is re-analysis of the MT data from SNORCLE Corridor 2 including application of depth-dependent dimensionality and strike assessment, updated 2-D inversion of edited data MT sets, and integrated geological and geophysical interpretation. We present the first 2-D resistivity images of the eastern part of the corridor (Corridor 2B) that crosses the North American Miogeocline and images Proterozoic rocks at the margin of Ancestral North America. We also update earlier results for the Cordilleran part of the corridor (Corridor 2A) given in Wennberg (2003) and Jones et al. (2005b).

2. Geological and geophysical background

2.1. Tectonic and geological setting

The Canadian Cordillera includes an east-verging fold and thrust system in the Rocky Mountain foreland, a west-verging thrust system to the west, and a large intermontane region (Cook et al., 2012). The eastern margin of the Cordillera is defined by the Cordilleran Deformation Front (CDF; Fig. 1), the eastern limit of the Cordilleran deformation. The current study area extends from the foreland to the intermontane region crossing the Foreland, Omenica, and Intermontane morphogeological belts (Monger, 1989). Along Corridor 2, the Foreland Belt consists of North American platform and basinal rocks, the Omenica Belt consists of the Cassiar, Slide Mountain and Yukon-Tanana terranes, and the Intermontane Belt includes the Quesnel, Cache Creek, and Stikine terranes (Fig. 1).

The eastern part of the study area is part of Ancestral North America (Laurentia) and includes the western margin of the North American craton and its cover, and ancestral continental shelf (miogeoclinal) platform and basin sequences (Fig. 1, Nelson and Colpron, 2007). The oldest sedimentary rocks in the region include Paleoproterozoic rocks of the Fort Simpson and Wernecke basins, which have been studied north of the current study area, and record a continental margin on the edge of the Wopmay orogen at around 1.8 Ga (Cook et al., 2012). The age of the Wernecke Supergroup is post-1.84Ga and pre-1.71 Ga (Nelson and Colpron, 2007). These rocks are overlain in places by the 1.0–0.78 Ga Mackenzie Mountain Supergroup (Thorkelson et al., 2005). Within the study area, Paleoproterozoic sedimentary rocks outcrop in the Muskwa anticlinorium just south of Corridor 2 (Fig. 1). The age of these rocks is bracketed between 1.77 Ga and 0.779 Ga. Although this age range overlaps with that of the Wernecke Supergroup, the stratigraphy differs (Nelson and Colpron, 2007). The slightly-metamorphosed Muskwa assemblage rocks have a composite thickness of 5.4 km (Nelson and Colpron, 2007; Cook et al., 2012).

Rocks of northwestern North America are interpreted to have undergone extensive deformation between 1.6 Ga and 0.8 Ga (Cook and Erdmer, 2005). Rifting occurred in the Neoproterozoic forming the northwest margin of Laurentia (Mortensen et al., 2006). During this rifting, or in a subsequent passive margin setting, sedimentary rocks of the 750–550 Ma Windermere Supergroup were deposited over a large area. The Proterozoic rocks are interpreted to extend in the sub-surface to large distances east and west of their surface exposure (e.g., Cook et al., 2004; Evenchick et al., 2005; Cook et al., 2012; Hayward, 2015).

The eastern part of the Canadian Cordillera is divided into block segments with contrasting geometry by a series of prominent northeast trending linear features interpreted to reflect the position of ancestral faults (Cecile et al., 1997; Hayward, 2015). The geometry of the Neoproterozoic asymmetric rifting differed between these blocks and resulting structures have influenced subsequent depositional and accretionary processes (Lister et al., 1986; Hansen et al., 1993; Cecile et al., 1997; Cook et al., 1999; Cook et al., 2005; Lund, 2008; Haywood, 2015). In the study area, the Liard Line (Cecile et al., 1997) shown on Fig. 1 separates the Blackwater Block to the northwest from the Macdonald Block to the southeast (Cecile et al., 1997; Haywood, 2015). In the Blackwater Block, rifting occurred on the lower plate and lower plate margins typically form broad continental margin (Fig. 2). Listric faults fragment and rotate upper crustal blocks which are then overlain by thick sedimentary sag basins (Lister et al., 1986; Hayward, 2015). In the Blackwater Block, and the Mackenzie Block to the northwest, the lower plate rift geometry has led to the formation of the broad Selwyn Basin (Fig. 1) and its thick deposits of Cambrian sedimentary rocks. In contrast, to the southwest rifting occurred in the upper plate and such rift margins produce narrow continental margins and thick continental crust (Lister et al., 1986). The narrow Kechika Trough (Fig. 1), which contains a relatively thin sequence of Cambrian sedimentary rocks, and the deflection of the basin to platform transform transition near the Liard Line, reflect the change rift geometry (Hayward, 2015).

In the SNORCLE study area the Omenica Belt contains pericratonic, para-autochthonous terranes related to Ancestral North America (e.g., Nelson and Colpron, 2007). The Cassiar terrane (cream colour, Fig. 1) has been displaced and transported northwards along the Tintina Fault (Monger, 1989). It contains Precambrian to Devonian platformal carbonate, sandstone, and shale. Rocks of the Kootenay terrane (purple colour, Fig. 1) resemble those of Ancestral North America but contain no record of Palaeozoic deformation and intrusion (Monger, 1989). The Slide Mountain oceanic terrane (grey colour, Fig. 1) is the western margin of the pericratonic, para-autochthonous terranes. The rocks of this terrane are derived from a marginal ocean basin (Colpron et al., 2006; Nelson and Colpron, 2007; Colpron and Nelson, 2009). The Yukon-Tanana terrane contains heterogeneous polydeformed metamorphic rocks of continental margin affinity as well as continental and back arc rocks that are interpreted to have formed on rifted basement of the Ancestral North American margin (Colpron et al., 2006; Nelson and Colpron, 2007; Colpron and Nelson, 2009).

The Intermontane Belt includes accreted terranes (Fig. 1). The Stikine terrane (Stikinia) (teal colour in Fig. 1) and the Quesnel terrane (Quesnellia) (orange colour in Fig. 1) are Devonian through Jurassic arcs and the Cache Creek terrane (tan colour in Fig. 1) preserves a relict fore-arc assemblage that contains slivers of high-pressure metamorphic rocks. Mihalynuk et al. (1994) and Nelson et al. (2006) propose that prior to accretion, the terranes formed an oroclinal bend with the Yukon-Tanana, Stikine, and Quesnel terranes enveloping the Cache Creek terrane. Stikinia records significant Mesozoic development. In Early to lower Middle Jurassic time, the Upper Hazelton Group and Iskut River Formation were deposited in an extensional environment including in the Eskay rift belt (Fig. 1; Gagnon et al., 2012; Barresi et al., 2015) which hosts important mineral deposits including porphyry style deposits and volcanogenic massive sulphide deposits (Nelson and Colpron, 2007). In Middle Jurassic to Cretaceous time marine clastic rocks were deposited in the Bowser Basin (Monger, 1989). Analysis of aeromagnetic data reveals that the basin is < 3 km deep near sites sno211 and sno212 and becomes shallower (1–2 km) north to site sno220 (Lowe, 1999) and interpretation of seismic reflections results indicates similar basin thickness (Evenchick et al., 2005).

The present configuration of the Cordillera arose during periods of crustal shortening in the Middle Jurassic-Lower Cretaceous and the late Cretaceous-Paleocene. A number of the terranes boundaries in the Cordillera are formed by accretionary thrust faults, such as the King Salmon Fault that emplaced the Cache Creek terrane onto Stikinia (Evenchick et al., 2005), but a larger number of boundaries formed during the Cretaceous and Cenozoic transcurrent faulting that led to orogen parallel translation of the various terranes (Gabrielse et al., 2006).

The Tintina Fault-northern Rocky Mountain Trench is a 2000 km long dextral transcurrent fault (Gabrielse et al., 2006; Hayward, 2015). Where crossed by Corridor 2 the fault is often called the Northern Rocky Mountain Trench (e.g., Snyder et al., 2005; Gabrielse et al., 2006) but herein we will refer to it as the Tintina Fault. Offset on the fault at 60°N and farther north has been estimated at ~490 km (Hayward, 2015). In the study area, rocks to the northeast of the Tintina Fault are dominantly the basin and platform sedimentary rocks of the Ancestral North American margin whereas rocks to the southwest are associated with the pericratonic and accreted terranes (Fig. 1). The Kechika Fault is related to the Tintina Fault system. A network of late Early Cretaceous orogen parallel strike slip faults includes the Teslin Fault and its southern extension, the Thibert Fault (Snyder et al., 2005), and the Kutcho Fault (Gabrielse et al., 2006).

2.2. Seismic surveys and analyses

Results of SNORCLE surveys are described in Snyder et al. (2009),

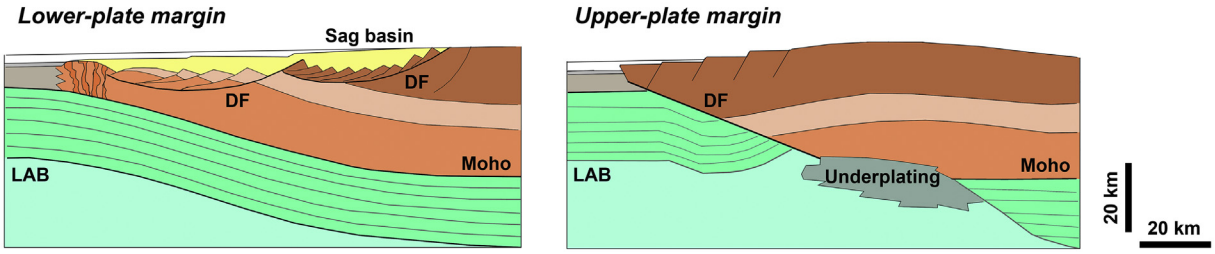

Fig. 2. Models of lower plate and upper plate rifting (modified from Lister et al., 1986; Péron-Pinvidic et al., 2015). Abbreviations: DF = Detachment fault; LAB = lithosphere-asthenosphere boundary. The models are both shown with the continent to the right to match the present day eastern position of Ancestral North America. The Blackwater Block and Mackenzie Block to the north of the Liard Line (Fig. 1) have characteristics of a lower-plate margin while the Macdonald Block to the south of the Liard Line has characteristics of an upper-plate margin. Crust to the east of the Tintina Fault, translated northwards along the fault, is also interpreted to be associated with an upper-plate margin.

Cook et al. (2012), Hayward (2015), Calvert (2016), and papers in the 2005 special volume of Canadian Journal of Earth Sciences (Cook and Erdmer, 2005). There have also been more recent geophysical studies in the northern Cordilleran region, including teleseismic studies (e.g., Courtier et al., 2010; Audet et al., 2016; Zaporozan et al., 2018; McLellan et al., 2018) and integrated geophysical and geodynamic studies, including of neotectonic processes (e.g., Mazzotti et al., 2008; Leonard et al., 2008; Hyndman, 2010, 2017; ten Brink et al., 2018).

In this study the focus is on SNORCLE Corridor 2 but results from Corridors 3 and 5 are discussed (Fig. 1). The east end of Corridor 2 (Corridor 2B) is in the western Canada Sedimentary Basin on rocks of the North American craton (Fig. 1). The profile extends northwest across platform and Kechika Basin rocks, crossing the Liard Line. After intersecting the Tintina Fault, Corridor 2A extends south across peri-cratonic terranes and onto accreted terranes of the Intermontane Belt. Corridor 3 extends from its northeast end in the Selwyn Basin to the Tintina Fault. It then extends to the southeast, and along with Corridor 5, crosses many of the same terranes as Corridor 2, before terminating to the west of the Intermontane terranes.

2.2.1. Corridor 2B

Along the eastern part of Corridor 2B, reflection and refraction results indicate flat-lying Mesozoic and Palaeozoic sedimentary rocks of the Western Canada Sedimentary Basin extend to depths of 2 to 5 km (Fig. 3; Cook et al., 2004; Fernández-Viejo et al., 2005; Clowes et al., 2005). Based on potential field trends and seismic results from SNORCLE Corridor 1, extending from the Slave Craton to the foreland, the near-surface sedimentary rocks, are interpreted to overlie rocks of the westward-thickening (1.5–3 s) Fort Simpson Basin (Cook et al., 2004; Lynn et al., 2005). The upper crust of this region is characterized by low P- and S-wave velocities (Fig. 3; Clowes et al., 2005; Fernández-Viejo et al., 2005).

Seismic trends are interrupted at the Muskwa Anticlinorium (Fig. 3) where west-dipping seismic reflections, that can be traced to the lower crust, indicate Muskwa Assemblage rocks have been brought to the surface along westward dipping thrust sheets (Cook et al., 2004; Snyder et al., 2009; Hayward, 2015). The upper crust is characterized by high seismic velocity (Clowes et al., 2005; Fernández-Viejo et al., 2005) and some interpretations suggest that older crystalline rocks have also been brought to shallow depths (Evenchick et al., 2005). In the western part of Corridor 2B, beneath exposures of Neoproterozoic Windermere rocks, east and west dipping reflections are observed at times of < 4 s and large-scale geological trends are interpreted to be sub-horizontal, implying Proterozoic rocks extend westward in the sub-surface.

Seismic results, such as deep penetrating reflections extending to surface Muskwa rocks, have been used to support the interpretation that the deeper parts of the crust beneath Corridor 2B are Proterozoic in age (e.g., Cook et al., 2004; Evenchick et al., 2005; Snyder et al., 2009; Hayward, 2015). However, as reviewed in Cook and Erdmer (2005), there are differences in the interpretation of the results and some authors attribute some of the reflection layering to ductile flow fabrics (Hyndman, 2017). Cook et al. (2004) and Snyder et al. (2002, 2009) interpret the middle and lower crust to the east of the Tintina Fault as being of 1.8–1.2 Ga age corresponding to Muskwa Assemblage rocks and possible underlying Wernecke Supergroup rocks. These parts of the crust are labelled A in Fig. 3. In contrast, Evenchick et al. (2005) interpret the rocks to be > 1.8 Ga crystalline basement rocks, potentially associated with the Wopmay orogen. There are also differences in the interpretation of the overlying parts of the crust (labelled B in Fig. 3). Cook et al. (2004) interpret these rocks to be of 1.2–0.8 Ga in age, corresponding to the Mackenzie Mountain Supergroup, whereas Evenchick et al. (2005) prefer an interpretation in which the rocks are Windermere Supergroup rocks overlying a relatively thin sequence of Muskwa Assemblage rocks. Although, the large-scale structure is dominated by sub-horizontal layering it is of note that in the area to the east of the Tintina Fault the middle to lower crust (> 10 km depth) is characterized by prominent east-dipping reflections (Cook et al., 2004; Evenchick et al., 2005; Clowes et al., 2005). A similar pattern is observed on Corridor 3. These features suggest the possibility of more complex structures than those included in the earlier interpretations.

2.2.2. Corridor 2A

Seismic reflection results from the Omenica and Intermontane belts on Corridor 2A provide evidence for complex upper crustal structure and more laterally uniform lower crust. At depths exceeding 12 km, crust west of the Tintina Fault is characterized by a westward tapering wedge of high reflectivity with some similarities to features on the east side of the fault. The wedge pinches out in the lower crust 300 km west of the Tintina Fault beneath Stikinia (Cook et al., 2004; Evenchick et al., 2005; Snyder et al., 2009; Cook et al., 2012; Calvert, 2016). Seismic reflection results indicate that the wedge contains layered rocks, but also a number of large-scale internal features including a synform between the Tintina Fault and Kechika Fault (Cook et al., 2004; Evenchick et al., 2005). Based on the correlations across the Tintina Fault, the westward tapering zone is interpreted as representing Proterozoic supracrustal rocks indicating that Ancestral North American rocks extend far to the west of the Tintina Fault (Cook et al., 2004; Evenchick et al., 2005; Snyder et al., 2009; Cook et al., 2012). As with the crust to the east of the Tintina Fault, there are differences in the interpreted age of rocks in the westward tapering wedge with Cook et al. (2004) and Snyder et al. (2002, 2009) interpreting the rocks as being of 1.8–1.2 Ga age and Evenchick et al. (2005) interpreting the rocks to be > 1.8 Ga crystalline basement.

Shallow reflectors along SNORCLE Corridor 2A can be correlated with the surface geology (e.g., Cook et al., 2004; Evenchick et al., 2005; Calvert, 2016; Cook et al., 2012). The results indicate that many of the terranes observed at the surface have been detached from their lower crust and occur as thin flakes overlying older crustal units. The westward tapering wedge is interpreted to have acted as a major tectonic accretion surface (Cook et al., 2004; Evenchick et al., 2005). The depth

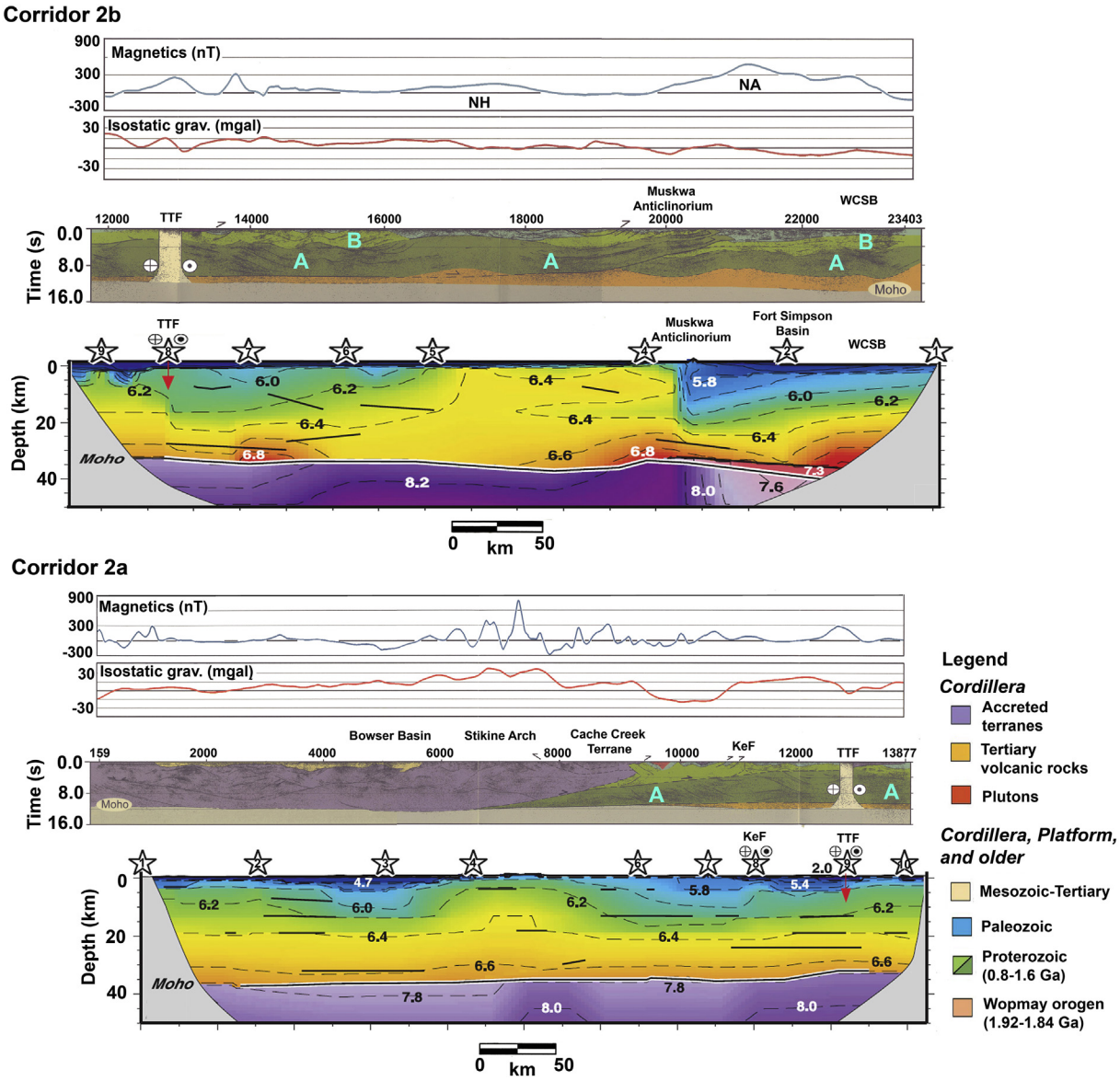

Fig. 3. Synthesis of seismic and potential field results for SNORCLE Corridor 2. The upper panel for each of corridor shows the magnetic and isostatic gravity anomaly (modified from Lynn et al., 2005), the middle panel shows the interpreted seismic reflectivity (modified from Lynn et al., 2005) with the legend showing the colour scheme, and the lower panel shows the P-wave seismic refraction velocity model and interpreted wide-angle reflections (modified from Clowes et al., 2005). The horizontal scale for the seismic reflection differs slightly from the seismic refraction because the reflection data is for the along-line distance. Numbers above the seismic reflection panels are vibration points (VP), stars above seismic refraction panels are shot points. Fig. 1 shows the map location of the VPs. Teal colour labels A and B denote parts of the crust for which the interpretations of the age of the Proterozoic rocks differs significantly in different studies (e.g., Cook et al., 2004; Evenchick et al., 2005). Note the prominent westward tapering wedge of reflectivity to the east of the Tintina Fault on Corridor 2A. Abbreviations: TTF = Tintina Fault Zone, KeF = Kechika Fault, NH = Nahanni Magnetic High, and Na = Natla Magnetic High. (For interpretation of the references to colour in this figure legend, the reader is referred to the web version of this article.)

to the base of the accreted terranes is uncertain and they may overlie, and at depth they may be interleaved with, Neoproterozoic (Windermere) rocks, Palaeozoic rocks and possibly older Proterozoic (Muskwa) rocks and Precambrian basement (Evenchick et al., 2005).

Cook et al. (2004), Evenchick et al. (2005) and Calvert (2016) provide interpretations of the weakly reflective uppermost crust. Immediately west of the Tintina Fault the variably reflective rocks beneath the surface Cassiar terrane are interpreted to indicate structurally-thickened Palaeozoic and Neoproterozoic Windermere strata. The Slide Mountain terrane and Yukon Tanana terrane in the Sylvester Allochthon (SA in Fig. 1) are strongly reflective and form a klippe extending to 3–5 km depth (Evenchick et al., 2005). The Cache Creek terrane is characterized by reflections with a flattened synformal pattern and a base at about 4 km (Calvert, 2016). The interpretation of Quesnellia and the Yukon-Tanana terrane, which form the surface exposure between the Cache Creek terrane and Cassiar Batholith, is more uncertain. The base of Quesnellia is sometimes defined by shallow reflections at 3 km depth (Cook et al., 2004; Evenchick et al., 2005) but deeper reflections suggest that the unit may extend into the middle crust beneath the Cache Creek terrane (Calvert, 2016). Interpretation of the structure of Stikinia is made more challenging by the Bowser Basin rocks overlying much of the terrane and by the complex deformation of the rocks (Cook et al., 2004; Evenchick et al., 2005).

Seismic reflection data also provide constraints on fault geometry. The Tintina Fault Zone is imaged on Corridor 2 as a 15 km to 25 km wide zone of weak and discontinuous reflectivity extending to a depth of at least 33 km (Cook et al., 2004; Evenchick et al., 2005; Snyder et al., 2005). Detailed studies of the fault on corridors 2, 3 and 5

indicate the fault zone broadens in the upper 5 km, thins in the middle crust, and widens again in the lower crust above the Moho (Snyder et al., 2005). The seismic reflection results suggest that other major transcurrent faults in the study area including the Kechika, Kutcho and Teslin-Thibert Faults do not penetrate deep into the crust (Cook et al., 2004; Evenchick et al., 2005; Snyder et al., 2005; Calvert, 2016).

2.3. Previous and related magnetotelluric studies

MT recordings were made on SNORCLE corridors between 1996 and 2000 using broadband (BBMT) and long-period (LMT) instruments. Jones et al. (2005b) review MT studies completed in the SNORCLE project and earlier results for different parts of the Cordillera and adjacent Proterozoic units are given in Wolynec (2000), Ledo et al. (2002a), Wennberg (2003), Ledo et al. (2004), Wu et al. (2005), and Ledo and Jones (2005).

MT results from the southwest Slave craton indicate crustal resistivity values in Mesoarchean Archean crystalline crust of > 40,000 Ω·m (Jones and Ferguson, 2001). This response can be attributed to an absence of conducting constituents such as graphite, sulphides, iron oxides and fluids (e.g., Duba et al., 1994; Yang, 2011; Evans, 2012; Selway, 2014). Neoarchean crust is also often very resistive, e.g., as observed in the Canadian Precambrian shield in parts of the Superior craton (Ferguson et al., 2005; Adetunji et al., 2014; Jones et al., 2014) and Rae craton (Spratt et al., 2014) but it may have laterally extensive conductive regions in the lower crust e.g., in parts of the Superior craton (Boerner et al., 2000), Hearn craton (Nieuwenhuis et al., 2014) and Rae craton (Spratt et al., 2014) as well as more localized zones of enhanced conductivity in supracrustal rocks and shear zones. Jones and Garcia (2006) determined resistivities of < 2000 Ω·m in the Yellowknife Greenstone Belt of the Slave craton.

On a global scale Proterozoic crust contains prominent crustal conductors. The crust in the Wopmay origin exhibits variable resistivity. A mid-crustal conductor was interpreted as being due to metamorphosed oceanic rocks accreted during the early stages of the collisions between two terranes (Wu et al., 2005). The Fort Simpson basin was imaged as a relatively resistive feature (> 1000 Ω·m) overlying more conductive crust of the Fort Simpson terrane (130–250 Ω·m). More generally, Boerner et al. (1996) indicate that euxinic sediments deposited in Paleoproterozoic foredeep settings are particularly likely to form significant conductive anomalies. Appropriate deformational and metamorphic conditions are needed to form very large-scale anomalies (Jones et al., 1997; Gowan et al., 2009).

Ledo et al. (2004) describe MT results from Corridor 3. The data define a fairly consistent geoelectric strike direction of N45°E parallel to the large-scale Cordilleran tectonic trends. Two-dimensional inversion of the MT data produced the resistivity model shown in Fig. 4 and reveals a number of conductors in the upper crust on the northeastern end of the corridor and in the mid-crust below the Cordillera. Shallow conductors (< 5 km depth) near the northeastern end of the profile were attributed to carbonaceous shales of the Selwyn basin. Other conductors all lie close to the upper surface of the westward tapering wedge of reflective rocks and were interpreted by Ledo et al. (2004) as being associated with the deformation that occurred during thrusting of younger rocks over the Proterozoic wedge. Ledo et al. (2002a) describe unconstrained 2-D inversions of the MT data collected on corridors crossing the Tintina Fault. The results reveal a similar structure of the fault zone on all profiles that includes, in contrast to many faults zones (e.g., Ritter et al., 2005), a resistive middle to lower crust.

The upper crust of the northern Cordillera is geophysically complex and the middle to lower crust is more spatially uniform (Fig. 4). MT results from the southern Canadian Cordillera show similar levels of complexity (Jones and Gough, 1995; Ledo and Jones, 2001) although in that location there are more faults extending into the lower crust and a regional variation in the conductivity of the mid to lower crust of the Omenica Belt can be correlated with Eocene extension. A number of deeper penetrating MT studies have also been conducted in the Canadian Cordillera and adjacent areas to image large-scale variations in resistivity and geometry of the mantle lithosphere (e.g., Soyer and Unsworth, 2006; Rippe et al., 2013; Meqbel et al., 2014; Bedrosian and Feucht, 2014).

Previous analyses of MT data from SNORCLE Corridor 2 have included dimensionality analysis and unconstrained 2-D inversion of data from Corridors 2A and 5 (Wennberg, 2003). Data from Corridor 2 have also been included in the large-scale synthesis studies of Jones et al. (2005b) (see Fig. 4) and Jones et al. (2014). The current study is intended to provide a more detailed analysis of the results for the whole of Corridor 2. As determined by Wennberg (2003), the MT data from Corridor 2 are complex in terms of dimensionality and strike adding to the motivation to re-examine the data with careful analysis, modelling and interpretation. In this study we include detailed unconstrained 2-D inversion of the MT data and geological constrained 2-D inversions. This approach makes optimum use of the closely-spaced, approximately 1-D, spatial distribution of the MT sites and will serve as critical platform for future 3-D inversions of a decimated data set.

3. SNORCLE Corridor 2 MT survey

The Corridor 2 MT dataset comprises 69 MT sites along the 800 km long profile. The corridor follows two of the widely-spaced highways through the region. Although the highways provide a crossing of the major geological units, significant lengths of the profile do not have an optimal orientation and are parallel to the strike of the Cordilleran terranes. MT acquisition consisted of broadband MT (BBMT) recordings at every site with average site spacing of approximately 12 km and a maximum spacing of 15 km. Long-period MT (LMT) recordings were made at every second BBMT site. The BBMT acquisition used Metronix ADU-06 instruments installed for 2–3 nights to acquire data in the period range 0.001 s to 1000 s. The LMT acquisition used LIMS instruments installed for 4 weeks recording to acquire data in the period range 20–10,000 s (Jones et al., 2005b). MT impedance responses were computed using robust spectral methods and remote referencing in order to reduce the influence of noise on the responses (e.g., Jones et al., 1989; Chave, 2012). MT acquisition included measurement of the vertical magnetic field. However, the quality of tipper responses obtained from the BBMT recordings was poor so the focus of the current study is on the MT data.

The MT impedance tensor contains four transfer functions relating horizontal components of the electric field to horizontal components of the magnetic field as a function of period. Individual impedance terms can be examined in terms of corresponding apparent resistivity and impedance phase (e.g., Vozoff, 1991). Phase depends on the change of apparent resistivity with period. In a horizontally-layered structure, at periods for which apparent resistivity is increasing with period (resistivity increasing with depth) phase is between 0° and 45°, and at periods for which apparent resistivity is decreasing with period (resistivity decreasing with depth) phase is between 45° and 90°. MT responses can be distorted by small-scale heterogeneities and in the simplest situation, called static shift, distortion will cause frequency-independent upward or downward shift of apparent resistivity. In this case, and for more complex distortion, the phase will provide a more robust indication of the regional MT response (e.g., Jones, 2012).

For 2-D and 3-D structures the apparent resistivity and phase are azimuthally-dependent. The derived impedance tensor can be used to determine the dimensionality of the response and, for 2-D structure, the geoelectric strike direction. For 2-D structures, the impedance mode corresponding to electric current flow parallel to strike is called the transverse electric (TE) mode and the mode corresponding to electric current flow perpendicular to strike is called the transverse magnetic (TM) mode. In complex environments it is sometimes useful to examine an azimuthally invariant impedance response such as the determinant response (Vozoff, 1991; Ledo and Jones, 2005).

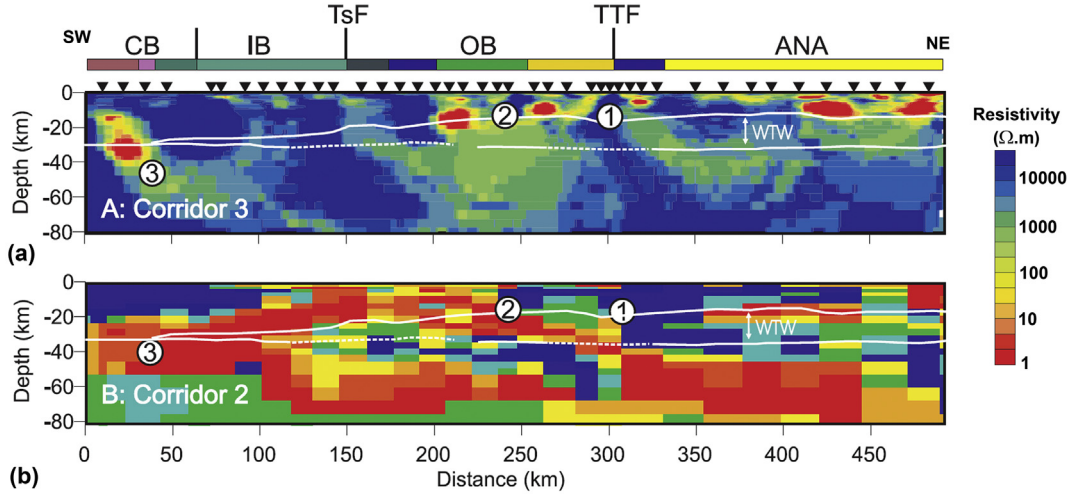

Fig. 4. Resistivity models for the northern Cordillera from previous studies (modified from Jones et al., 2005b). The upper panel shows the model for Corridor 3. Abbreviations: CB = Coast Belt, IB = Intermontane Belt, OB = Omenica Belt, ANA = Ancestral North America, TsF = Teslin Fault, TTF = Tintina Fault, WTW = westward tapering wedge. Numbered labels indicate prominent features: 1 = resistive crust beneath Tintina Fault, 2 = upper crustal conductors at 10–20 km depth above the westward tapering wedge, 3 = northeast-dipping conductor extending from the mid-crust deep into the lithosphere. The lower panel shows a lower resolution inversion model for Corridor 2 extracted from a larger synthesis model. The position of the WTW and labels indicating resistivity features have been projected from Corridor 2.

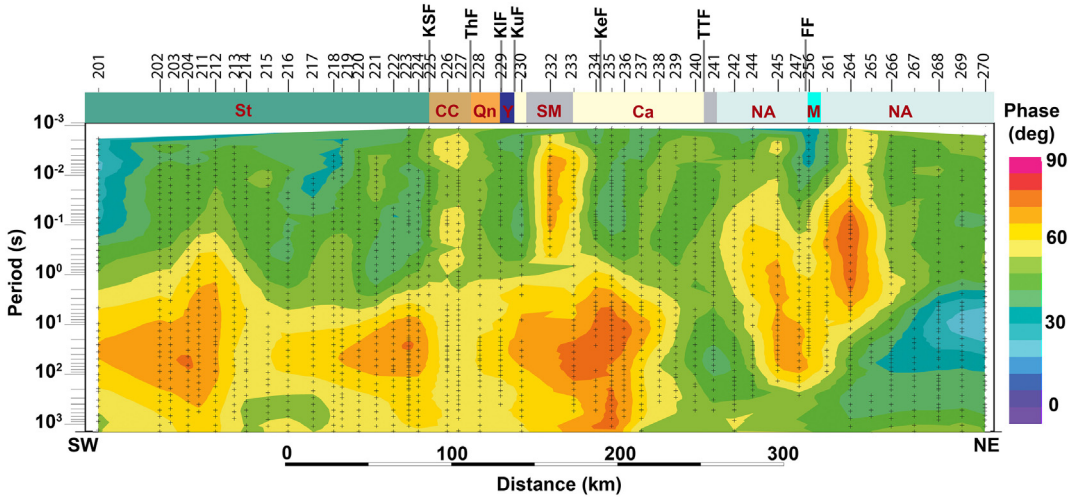

Fig. 5. Pseudosection of the determinant phase providing an overview of MT responses along Corridor 2. Sites have been projected onto a profile with an azimuth N45°W and some sites that were closely-spaced after projection have been excluded in order to yield a more uniform density. Crosses show the position of data points used in the contouring. Key: KSF = King Salmon Fault; ThF = Thibert Fault; KlF = Klinkit Fault; KuF = Kutcho Fault; KeF = Kechika Fault; TTF = Tintina Fault; FF = Forcier Fault; St = Stikinia; CC = Cache Creek; Qn = Quesnellia; Y = Yukon-Tanana; SM = Slide Mountain; Ca = Cassiar; NA = North America; M = Muskwa Anticlinorium.

The determinant phase pseudosection for Corridor 2 provides a first-order overview of the electrical resistivity variations along the profile (Fig. 5). Sites are projected onto a N45°E profile perpendicular to the large-scale NW-SE geological strike. Overall, the response shows significant complexity at short periods (< 1 s), e.g., with a number of responses observed at only two or three adjacent MT sites, reflecting the complexity of upper crustal structures. In contrast there is more spatial uniformity at longer periods (> 1 s) reflecting the greater uniformity in the middle to lower crust and upper mantle lithosphere. Conductors, inferred by high phase values in Stikinia, Cache Creek terrane, and Slide Mountain terrane, dominate the short period ($< 10^{-1}$ s) response on Corridor 2A whereas the Muskwa Anticlinorium overlies a locally resistive region (inferred by low phase values) on Corridor 2B. The Tintina Fault Zone (TTF in Fig. 5) has a relatively resistive response that extends to long periods. It separated a more conductive response with an eastward dip at intermediate periods (10^{-2}–10^{2} s) to the northeast from a conductive response at slightly longer periods (10^{0}–10^{3} s) to the southwest. Finally, there is a distinctive wedge-shaped region of low phase at longer periods (> 1 s) on the northwestern end of the profile.

4. Dimensionality and strike analyses

Noting the complexity of resistivity structure in the Cordillera seen in earlier MT studies (e.g., Wennberg, 2003) we apply multiple methods for dimensionality and strike analysis. As the first step, dimensionality of the Corridor 2 data was analyzed using WAL rotational invariants (Weaver et al., 2000) implemented with consideration of data errors in the WALDIM code (Martí et al., 2009). WAL-defined dimensionality for Corridor 2 is shown in Fig. 6. The results confirm the presence of complex structure with many sites exhibiting either a 3-D response or an indistinguishable 3D/2D response, particularly at longer periods (> 10 s). At shorter periods there are a number of smaller parts of the

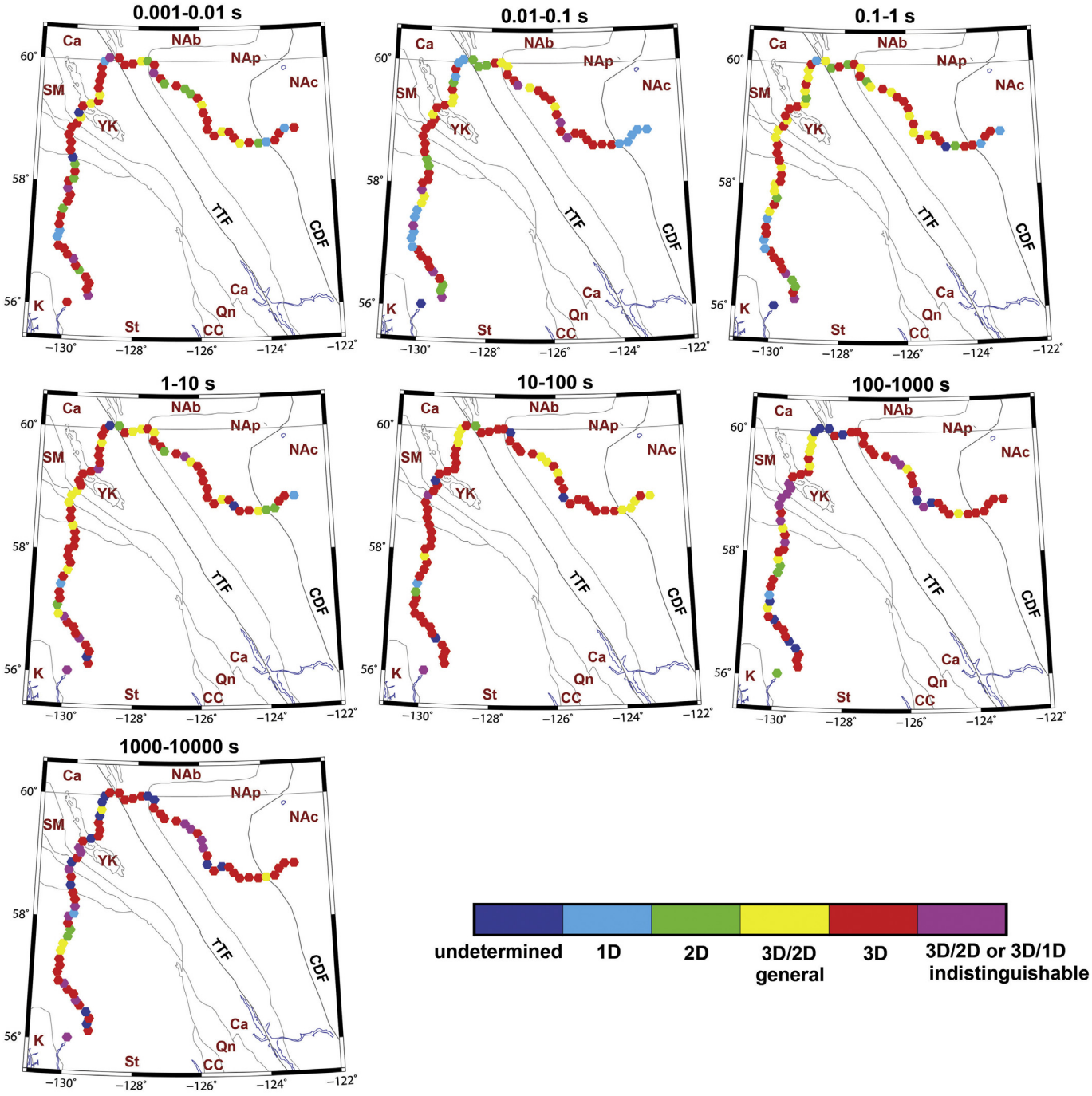

Fig. 6. Map of WALDIM results for different period bands.

profile, typically consisting of 3–6 adjacent sites, in which 1-D and 2-D behaviour is observed.

Groom-Bailey (GB) tensor decomposition (Groom and Bailey, 1989; Jones, 2012) of the data set confirms the presence of significant galvanic distortion. GB tensor decomposition seeks the best fit for a model of superimposition of localized 3D scatterers on a 1-D or 2D regional structure. Extended Groom-Bailey analysis (McNeice and Jones, 2001; Jones, 2012) using the STRIKE program, in a period band from 10^{-3}–10^{3} s, and with a strike angle of N45°W, shows 16 of the 69 sites have moderate to high shear (> 20° shear angle). The distortion is quite localized with a maximum of two adjacent sites yielding similar shear and twist values. However, several groups of five to six sites exhibit consistently high, but spatially varying, distortion indicate the presence of upper crustal lithology with greater resistivity heterogeneity.

The normalized root mean square (rms) misfit of the GB model provides a measure of three-dimensionality. For the GB analysis described above, and assumed 3% impedance errors, 19 of the 69 sites yielded rms misfits exceeding 3.0. This misfit mostly occurs at widely spaced individual sites although there is one group of three adjacent sites (sno-256-sno258) with rms misfit between 3.0 and 4.0, and several groups of two adjacent sites (sno236-sno237, sno244-sno245, sno264-sno265) with rms values exceeding 3.0. Overall, the GB analysis suggests three-dimensionality on Corridor 2 is due to relatively localized structures.

In this study we reanalyse strikes for all of Corridor 2 using three approaches: phase tensors (Caldwell et al., 2004; Booker, 2014), extended GB decomposition (McNeice and Jones, 2001), and the method of Becken and Burkhardt (2004). The phase tensor (PT) method allows

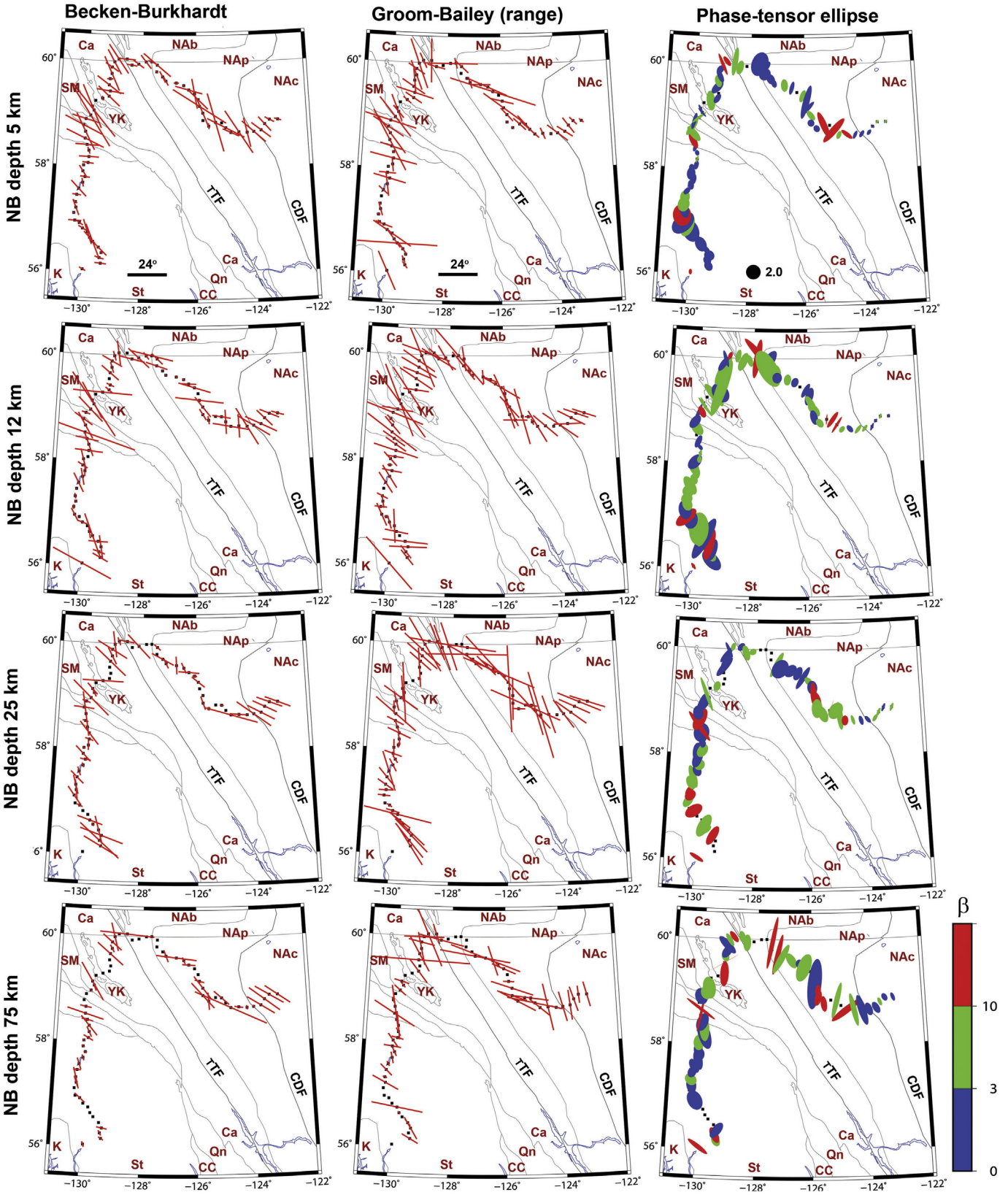

Fig. 7. Strike results for Niblett-Bostick depths of 5, 12, 25 and 75 km determined using Becken-Burkhardt (BB), Groom-Bailey (GB) and phase tensor (PT) methods. For the GB results, azimuths are plotted in the northwest quadrant and line length is proportional to the phase difference. For the BB method, azimuths are plotted in the northwest quadrant and line length is proportional to the difference between the ellipticities related to the two telluric vectors. For the PT results the long axis of the ellipse corresponds to the direction of maximum impedance phase, the ellipticity provides a measure of the strength of two-dimensionality and the ellipses are colour coded to show phase tensor skew β which provides a measure of the three-dimensionality. See text for additional details. See Figs. 1 and 4 for abbreviations. Additional abbreviations: K = Kootenay terrane; NAb = North America basin, NAp = North America platform, NAc = North America craton. (For interpretation of the references to colour in this figure legend, the reader is referred to the web version of this article.)

derivation of dimensionality and strike from the MT impedance tensor in a manner unaffected by distortion and requires no assumption about the dimensionality of the local and regional conductivity structure. However, PT responses are affected by errors in the impedance response, particularly in the case of strong distortion (e.g., Jones, 2012). The Becken and Burkhardt (BB) algorithm is based on the occurrence of linear polarization of the electromagnetic fields in the strike system. Ellipticities of telluric vectors, as manifest through the columns of the impedance tensor, are minimized to yield the strike angle (Becken and Burkhardt, 2004).

To account for the fact that sites may have very different electromagnetic penetration depths at similar frequencies, strikes are evaluated at Niblett-Bostick transformed depths (Niblett and Sayn-Wittgenstein, 1960; Jones, 1983; Miensopust et al., 2011) rather than at specified periods. Results for depths of 5, 12, 25 and 75 km, representative of upper, middle and, lower crustal and upper mantle depths respectively, are shown in Fig. 7. For the BB and PT strike results the depth transformation is based on the invariant or Berdichevsky response (the arithmetic average of the off-diagonal impedance terms) and the strike result is for the nearest depth-transformed depth value to the specified depth. For the GB strike results, the Niblett-Bostick depth transformation is based on the determinant response, and strike result is for a range of transformed depths centred on the specified value (1.6–8 km, 8–16 km, 16–35 km, and 35–250 km).

For the GB and BB methods, the 90° ambiguity in strike determination is addressed by plotting the azimuths in the northwest quadrant defined by the geological strike. PT results are plotted using the PT ellipse and for 2-D structures the longer axis will correspond to the direction of maximum impedance phase. This direction will correspond to the true strike for sites on resistive blocks adjacent to linear conductors but will be perpendicular to the true strike for sites on a conductive block adjacent to a resistive block (e.g., Hamilton et al., 2006). PT ellipticity provides a measure of the strength of the two-dimensionality and phase tensor skew β provides a measure of the three-dimensionality. Values of $|\beta| < 3$ mean off-diagonal terms of the phase tensor (which are zero in the 2-D case) are an order of magnitude smaller than the diagonal terms and is reasonably taken as the limit as quasi-two-dimensionality (e.g., Caldwell et al., 2004; Booker, 2014). $|\beta| < 10$ means the off-diagonal terms of the phase tensor are only a factor 3 smaller and is an overly liberal limit for quasi-two-dimensionality (Booker, 2014).

There are similar patterns for the strike azimuths along Corridor 2 for all three methods. Overall, most scatter is observed in the GB strike results, which could be due to the improper fit of the decomposition model and the presence of localized 3-D structures. There is significant variation in strike with location and depth but results centre on a value of N45°W. Rose diagrams of the GB results are shown in the Supplementary Material. Some PT azimuths are perpendicular to this angle, e.g., at 12 km depth at the east end of the profile and at 25 km depth on the North American platform, but these responses may be due to sites in conductive zones adjacent to structures with N45°W strike. The three-dimensionality indicated by the phase tensor is similar to estimates from the WALDIM and GB methods, for example showing localized patches of 3-D responses along the profile and an increase in three-dimensionality with depth. However, it is significant that many sites exhibit only moderate phase-tensor skew values (< 3°).

The broad-band induction arrow responses for the SNORCLE Corridor 2 data set are relatively noisy and erratic at periods shorter than 0.1 s. At periods longer than 10 s the broad-band and long-period induction arrows have a dominantly south-southwest azimuth, interpreted to be caused by the electromagnetic coast effect which can influence induction arrows to relatively large distances from coastlines. Induction arrows for periods of 0.1 to 10 s are shown in the Supplementary Material. The responses confirm the results of the MT dimensionality and strike studies. The arrow azimuth indicates a dominant N45°W strike, but there is considerable scatter indicating the presence of localized 3-D structures along the corridor.

The collective results of the dimensionality and strike analyses provide support for the validity of 2-D inversion of the Corridor 2 MT data. Careful strike analysis has yielded azimuths that are consistent between different methods, fairly consistent from site to site, and displaying alignment with larger-scale geological features. The observations suggest the presence of strong 2-D elements in the regional resistivity structure. The results support the use of a N45°W strike azimuth in the inversions with the MT TE mode corresponding to the N45°W direction and the TM mode to the N45°E direction. In earlier assessments, Ledo et al. (2004) determined an overall strike azimuth of N45°W for Corridor 3 and Wennberg (2003) determined an azimuth of N45°W for Corridor 2A at short and intermediate periods with a rotation to N60°W at long periods. The presence of 3-D components in the Corridor 2 dataset data set means that results of the 2-D analysis must be interpreted with care, and establishes justification for future 3-D modelling and inversion of the data set. However, 2-D distortion decomposition extracts the most 2-D information possible from the MT impedance tensors.

Phase difference between the TE and TM modes for 2-D, or approximately 2-D, structures provides an estimate of the strength of the resistivity structures present and is indicated in Fig. 7 by the length of the azimuth symbol. It is noticeable that there are some profile segments with much more prominent resistivity structure. These include: in the middle to lower crust at the southwest end of the profile in Stikinia; in the upper to lower crust crossing the accreted Cache Creek, Quesnel and Slide Mountain terranes; at crustal and lithospheric mantle depth near the Tintina Fault; near the Muskwa Anticlinorium; and in Ancestral North American rocks at the eastern end of the profile. These features correspond to resistivity signatures noted in the determinant phase pseudosection (Fig. 5). The Niblett-Bostick transformed results provide an estimate of the depth of these structures.

Geoelectric strike results show some correlations with features in gravity and magnetic data (Fig. 8). Detailed interpretations of potential field data sets can be found in Lynn et al. (2005) and Hayward (2015). The N45°W geoelectric strike is parallel to linear gravity and magnetic anomalies observed along the Tintina Fault Zone, intermediate wavelength features in the magnetic data to the southwest of the Tintina Fault (Fig. 8), and features in the short-wavelength filtered gravity response to the southwest of the Tintina Fault (Lynn et al., 2005). The increase in geoelectric two-dimensionality at the eastern end of Corridor 2B is spatially correlated with the south end of the major Fort Simpson gravity high (Lynn et al., 2005; Hayward, 2015) that can be traced to the north over a distance of at least 600 km. The Fort Simpson magnetic high trends just to the east of the east end of Corridor 2. The increase in two-dimensionality near the south end of Corridor 2 is also associated with a gravity high. In the gravity data the response of the Tintina Fault Zone is interrupted at the latitude of Corridor 2 by a NNE trending gravity high that separates lower gravity values in the Kechika and Selwyn Basins (Hayward, 2015). The MT strikes show no major perturbations at this location.

5. MT inversion

5.1. Inversion approach

MT data were inverted using 2-D methods in the dominant N45°W strike direction. Because of the increase in 3-D responses at long periods, inversions were focused on defining the crustal electrical resistivity structure. In the first phase of the inversions, data from Corridor 2A and several additional sites from Corridor 2B, included in order to lengthen the profile, were inverted. In the second phase, inversions were applied to carefully selected sites from Corridor 2B plus several additional sites from Corridor 2A. The projection of sites onto a modelling profile perpendicular to the N45°W strike makes some sites too close to each other and intercalates sites separated by considerable

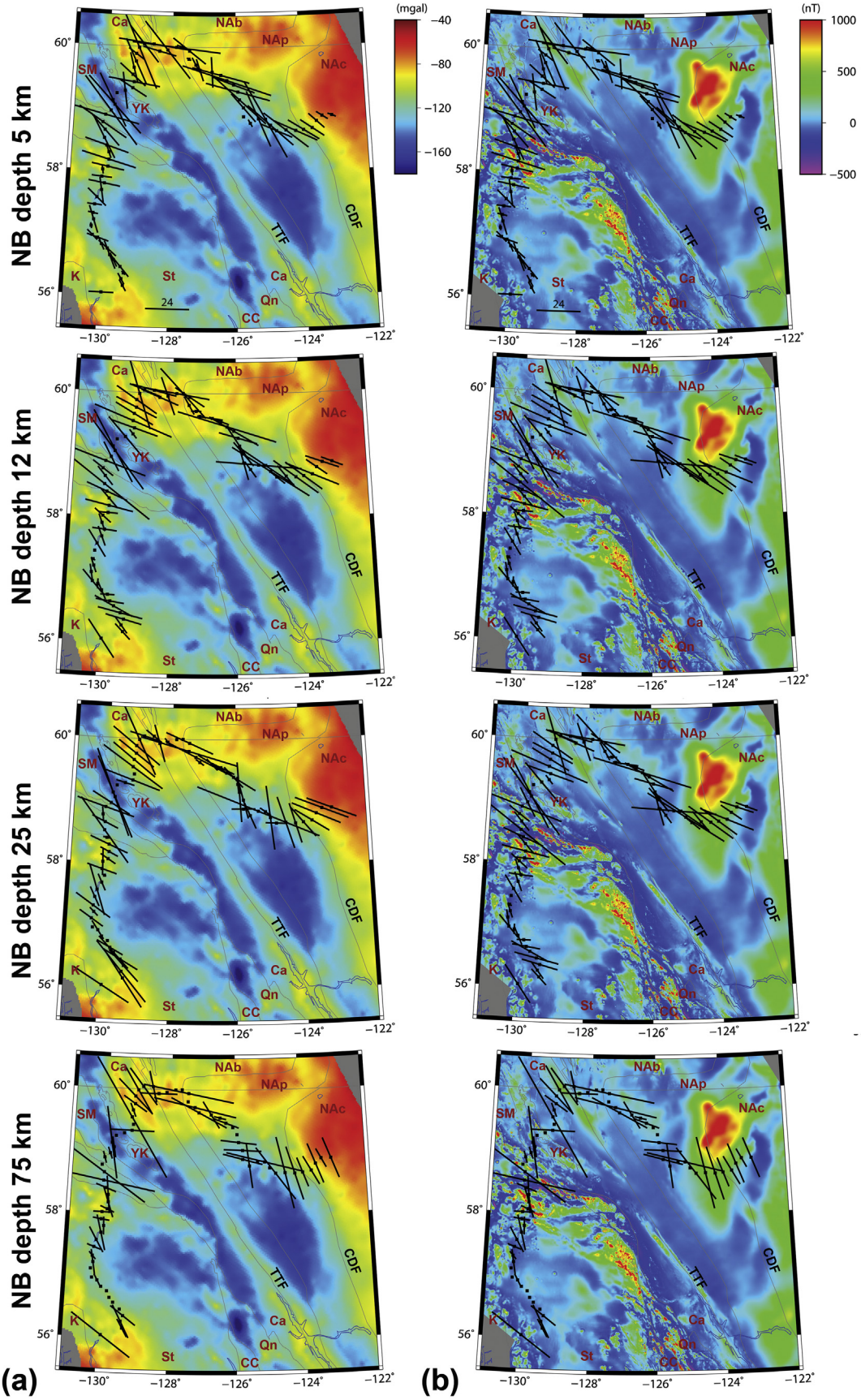

Fig. 8. Phase tensor strikes overlaid on potential field results. The phase tensor results are displayed using the azimuth of the axis of the phase tensor falling in the northwest quadrant and a length correspond to the phase difference in degrees of the major and minor phase tensor axis. Upper panels include a scale bar corresponding to a 24° phase difference. Left panels show the strike results overlaid on Bouguer gravity anomaly data from the Government of Canada 2 km Bouguer gravity anomaly grid. Right panels show the strike results overlaid on residual magnetic field data from the Government of Canada 200 m residual magnetic anomaly grid.

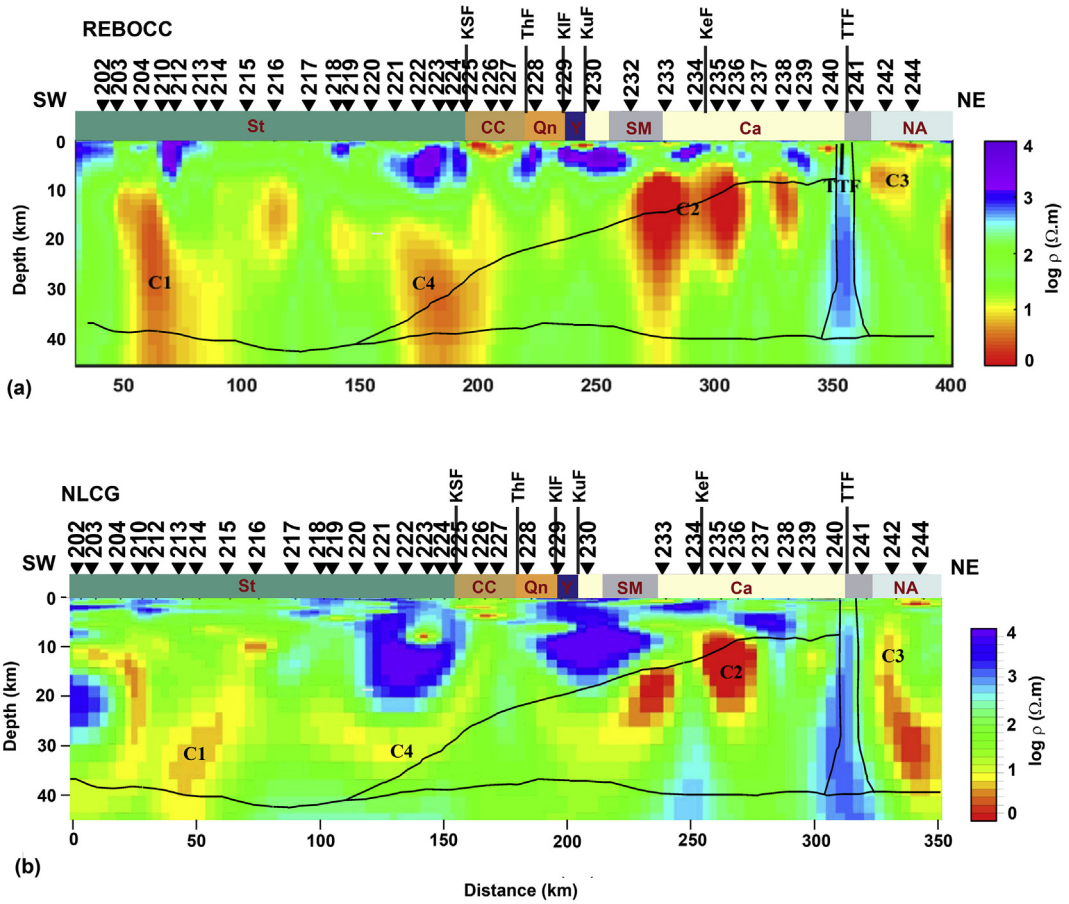

Fig. 9. (a) REBOCC and (b) NLCG two-dimensional model resulted from joint inversion of TE- and TM-mode data for Corridor 2a. The black lines superimposed on the model show the seismically-defined location of the Moho, the Tintina Fault Zone, and the westward tapering wedge of reflective rocks (Cook et al., 2004). Labelled resistivity features are discussed in the text. Note the slightly different colour scales for the two panels. (For interpretation of the references to colour in this figure legend, the reader is referred to the web version of this article.)

distance along-strike. Sites from short segments of Corridor 2A and from a long segment of Corridor 2B were culled severely so as to retain only more closely-spaced space sites in the inversions. Separate inversion of MT data from Corridors 2A and 2B is consistent with the contrasting geological structure on each corridor and different degree of site culling required for each corridor, facilitates comparison of MT results with other geophysical results presented for individual corridors (e.g., Cook et al., 2004; Evenchick et al., 2005; Clowes et al., 2005; Fernández-Viejo et al., 2005), expedited the inversion process, and reflects the evolution of the analysis.

In order to provide information on the resolution of the resistivity features, and to increase the reliability of the inversion results, two independent inversion approaches were applied. Both approaches used regularized 2-D inversions in which the algorithm minimizes an objective function that includes data residuals and second spatial derivatives with respect to resistivity structures. In the first approach, data the MT data were processed by the phase tensor method and then inverted using a 2-D REBOCC code (Siripunvaraporn and Egbert, 2000). In the second approach, data were processed using Groom-Bailey tensor decomposition and inverted using a Non Linear Conjugate Gradient (NLCG) code (Rodi and Mackie, 2001, 2012). Both approaches were applied to the Corridor 2A dataset. Only the NLCG approach was applied to the Corridor 2B data, but resolution information obtained from Corridor 2A inversions can be used in assessing the Corridor 2B inversion models.

In the first inversion approach, data for 0.004 s to 5000 s were considered, so as to maintain an appropriate period range to resolve crustal structure and to avoid three-dimensional effects in very long period data. Input data for the 2D inversion were corrected for distortion using the phase tensor method (Bibby et al., 2005) with a normalization based on the GB approach. Examples of the distortion corrected data are provided in the Supplementary Material. Prior to the inversions, data were edited to reduce the influence of sites with strongly 3-D responses and data points inconsistent with the D^+ criterion (Parker, 1980; Weidelt and Chave, 2012). A 100 Ω·m uniform half space was used as the starting model in the inversions. Correction of static shift effects was conducted using a manual approach between inversion runs and resulted in a slight decrease in the RMS misfit. A relative error floor of 20% and an absolute floor of 1.5° were selected for apparent resistivity and phase data, respectively. These values give priority to the phase response in order to overcome any uncorrected static shifts.

In the second inversion approach, the period range 0.001 s to 1000 s was considered. MT responses were obtained using the STRIKE program and a single-band fit to the observed impedances in the N45°W strike. Examples of the fitted GB 2-D regional responses are provided in the Supplementary Material. As with the first approach, data were edited to remove non-2-D responses. Additional editing was done between inversion runs to remove parts of the data set that could not be fitted by a 2-D resistivity model. A 100 Ω·m uniform half space was used as the starting model. Static shift was corrected used a similar method to the first inversion approach and was also included as a parameter in some inversion runs. Relative error floors of ρ_{aTE} = 48% and ρ_{aTM} = 24% were used for apparent resistivity (corresponding to impedance error floors of 24% and 12%) and absolute error floors of 1.7° and 0.9° were used for phase (corresponding to impedance error floors of 3% and

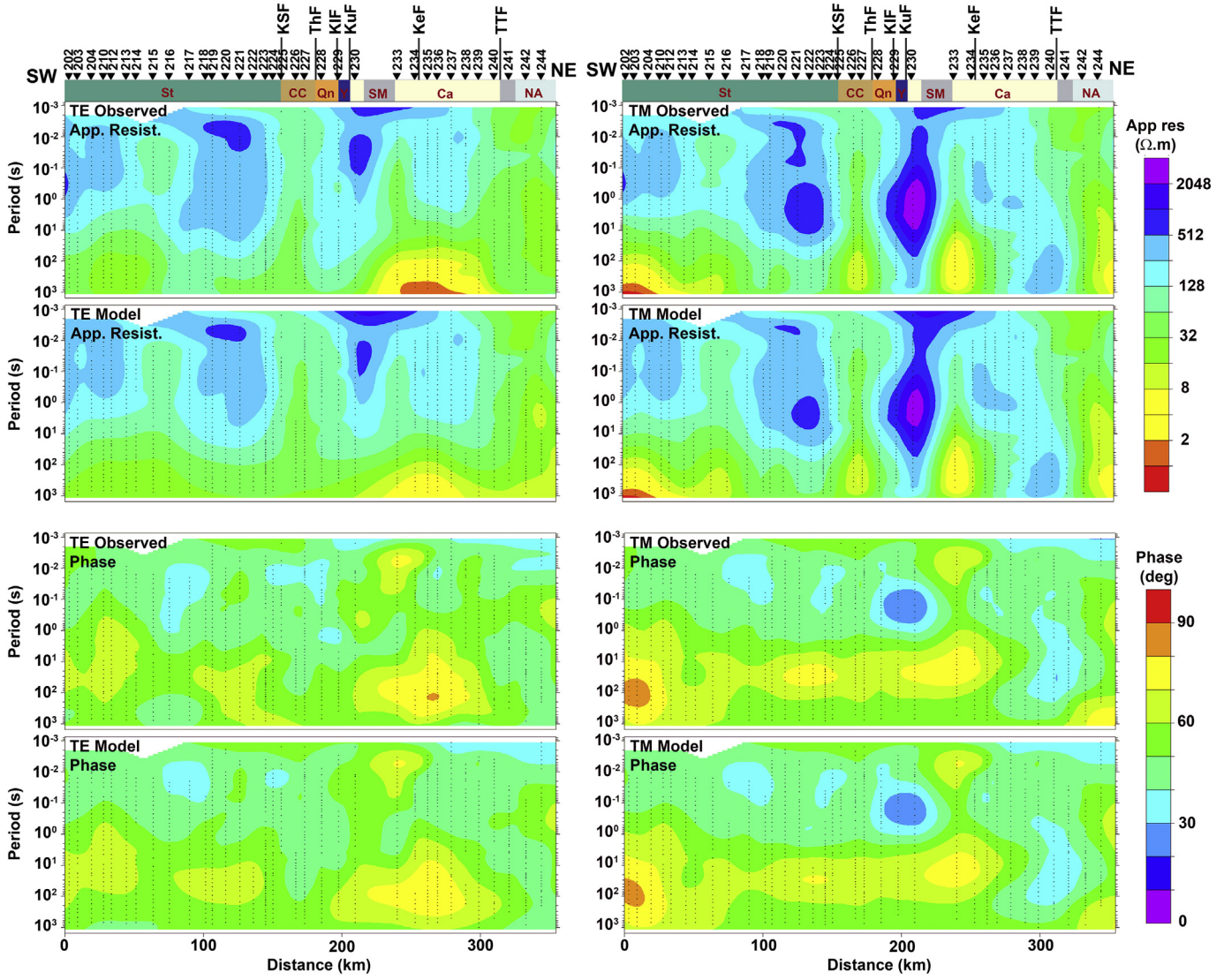

Fig. 10. Fit of the unconstrained NLCG inversion model to the observed data for the Corridor 2A inversion. The total normalized rms misfit for error floors applied (see details in the text) is 2.17. Left panels compare observed and model pseudosections of the apparent resistivity and phase response and right panels compare corresponding pseudosections for the TM response.

1.5%). As well as emphasizing the phase response the error floors gave priority to the TM responses. This weighting accommodates certain weak 3-D effects. For example, when the conductive features in a model have a finite strike length, the TE response is generally more distorted than the TM response (Ledo et al., 2002b; Ledo, 2006). However, there are some geometries for which the TM mode is more affected by 3-D effects (e.g., Park and Mackie, 1997). The NLCG inversion used a uniform grid Laplacian to define roughness, it minimized the absolute value of the Laplacian squared, and it used a regularization parameter of $\tau = 3.0$ (a value often adopted in inversions of data sets of similar scale).

5.2. Unconstrained inversions for Corridor 2A

Unconstrained 2D inversions of the Corridor 2A MT data were undertaken using both inversion approaches, examining the effect of different data components, separately and in combination. Models derived from joint inversion of TE- and TM-mode data using two inversion approaches for line 2a are shown in Fig. 9. The normalized rms misfits for the REBOCC and NLCG inversions and the error floors listed above were 3.15 and 2.17 respectively. Fig. 10 compares pseudosections of the observed data and model response for the NLCG inversion and additional information on model misfit is provided in the Supplementary Material. The inversion model reproduces all of the main responses observed in the data. Largest misfits are observed at long periods, reflecting the increase of the 3-D responses at these periods. There are also some differences between the observed data and model response observed at shorter periods e.g., in the TE phase response for the Cassiar and Slide Mountain terranes.

The main features defined in the two resistivity models are supported by both inversion approaches, by inversion of different components of the MT transfer functions, and can be inferred from examination of the observed MT responses (e.g., Figs. 5 and 7). However, there are some differences in the size and shape of the structures in the REBOCC and NLCG inversion models. For the model regularization used in the inversions, the NLCG algorithm produces larger vertical smearing of resistive features, e.g., beneath the Quesnel to Slide Mountain terranes whereas the REBOCC algorithm produces more smearing of conductive features e.g., conductors beneath the Slide Mountain and Cassiar terranes. The validity and resolution of the individual features of the model was also assessed through sensitivity analysis by using starting and/or reference models with the particular features excluded and

rerunning the inversion. Due to the masking effect of enhanced conductivity, the base of conductors is poorly resolved by MT, and the true depth extent of conductors may differ from that shown in Fig. 9 (see, e.g., Jones, 1999).

The upper 10 km of the resistivity models has a complex resistivity response indicating a heterogeneous upper crust. There are numerous resistive zones and several conductive zones that are evident in the same location in both the REBOCC and NLCG models, although these features sometimes have somewhat different size and shapes in the two models. The upper crust of Stikinia includes a number of resistive zones ($> 1000\,\Omega$·m) in a background of more moderate resistivity (30–300 Ω·m); the uppermost crust of the Cache Creek terrane includes a thin conductive zone ($< 10\,\Omega$·m); and the upper crust of the Cassiar terrane has a similar range of resistivity values to Stikinia. The Slide Mountain terrane includes very conductive rocks in the upper 10 km although these are not fully resolved in the inversion models because of the removal of data points exhibiting extreme distortion and departing from a 2-D response. In contrast, the determinant phase pseudosection in Fig. 5 shows the conductive response in the Slide Mountain terrane (as well as in the Cache Creek terrane) very clearly at the shortest periods.

The resistivity models contain a number of important larger-scale features. In both sets of inversion results the Tintina Fault Zone is imaged as a relatively resistive ($> 300\,\Omega$·m) sub-vertical zone between sites sno240 and sno241 extending from 5 km depth into the lithospheric mantle. Highest resistivity values in this zone are observed at depths exceeding 15 km.

Both inversion models include a series of conductors (1–10 Ω·m), labelled C1 on Fig. 9, in the middle to lower crust of Stikinia near the southern end of the profile. This feature can be related to conductive response observed at intermediate periods in the determinant phase response (Fig. 5) as well as to the increased strike response seen at larger Niblett-Bostick depths (Figs. 7 and 8). The most conductive responses ($< 3\,\Omega$·m) are observed beneath sno204 and sno216. The REBOCC model suggests the two south features may connect to form a northeast dipping conductor that broadens into a moderately conductive zone ($< 10\,\Omega$·m) in the lower crust beneath sites sno210 to sno215. The lower crustal feature may also connect with the conductor beneath sno216 but the connection may be a consequence of the smoothing applied in the inversion. The resistivity models also suggest the conductive zones extend into the mantle. This aspect is assessed in constrained inversions described in the next section.

The inversion models also define a series of conductors with their tops located just above the west-tapering seismic wedge (labelled C4, C2 and C3) in Fig. 9: conductor C4 is in the lower crust beneath the northern part of Stikinia, conductor C2 is a two-lobed feature in the upper to mid crust beneath the Cassiar terrane, and conductor C3 is located in the upper crust to the east of the Tintina Fault beneath the rocks of the Kechika Basin. The shape of these conductors varies between the REBOCC and NLCG inversion models but the general position and resistivity values of the conductors is similar in both models. The relationship of these features to the westward tapering wedge is examined more closely in constrained inversions.

5.3. Constrained inversions for Corridor 2A

In the constrained inversions well-resolved parameters of the seismic models were included as independent constraints in the MT inversion to improve resolution of deep structures and the consistency of MT and seismic results. Information was introduced using tears in model regularization at locations of postulated boundaries, where a "tear" means that conductivity contrasts across the boundary do not contribute to the overall roughness so are not penalized. Additionally, resistivity values in parts of the inversion model were forced towards particular values (or "fixed") by including their weighted departure from a priori values as part of the objective function. Additional inversions were performed on the Corridor 2A data to introduce constraints related to the Moho, Tintina Fault and westward tapering wedge.

In the first constrained inversion, constraints related to the Moho and westward tapering seismic wedge are introduced. Although there are some local variations, the Moho depth for Cordillera is 33 ± 2 km (Hyndman, 2017) and in the present study the Moho was defined by a horizontal break in the smoothing constraints at 35 km depth. The westward tapering wedge was defined using seismic reflection results in Cook et al. (2004), Evenchick et al. (2005), and Calvert (2016). Although there are some differences in the interpretation of the upper surface of the wedge (e.g., Calvert, 2016) these have maximum offset of 6 km and at 20 km depth and are outside the resolution of the MT method. The boundaries of the wedge defined in Cook et al. (2004) were used to define a break in the smoothing in the inversion models. In the Cartesian meshes used in the inversions, the dipping surface was approximated by a series of steps.

Constrained inversions were conducted using both the REBOCC and NLCG approaches, starting from either an initial 100 Ω·m half-space or the model from an earlier inversion. Comparisons of the data fit at representative sites for the unconstrained and constrained models are provided in the Supplementary material. Fig. 11 shows the final model for a REBOCC inversion that included both Moho and wedge boundaries. The normalized rms misfit, based on the error floors above was 2.73 (compared with the result for the unconstrained inversion of 3.15). In the NLCG approach, the resistivity model included breaks in the smoothing at the Moho and margins of the seismic wedge and the resistivity within the wedge was additionally fixed to a value of 100 Ω·m (Fig. 11). The normalized rms misfit for the model, based on the error floors noted above was 2.21 (only 2% larger than the result for the unconstrained inversion of 2.17). Pseudosections of the constrained model response appear very similar to those for the unconstrained inversion (Fig. 10). Information on rms misfit at individual sites is included in the Supplementary material.

The most important result of the constrained inversions is that they show it is possible to fit the data to a similar level of misfit as unconstrained inversions with conductors C2, C3, and C4 lying above the west tapering wedge. The result for C3 is shown only in the REBOCC results in Fig. 11, because for the NLCG constraints, the tear at the surface of the wedge was not extended east of the Tintina Fault Zone. The results also show that the MT data are compatible with a resistivity model in which the westward tapering wedge has a uniform, moderate resistivity. The results of additional constrained inversions, not shown here, indicate that if the resistivity within the wedge is set to higher values, such as 1000 Ω·m, it is not possible to obtain a comparable level of fit to the data.

The constrained inversions also provide constraints on conductor C1 at the southwestern end of the corridor. The NLCG inversion model shows that the data are compatible with a model in which the conductor is confined to the crust. However, the NLCG and REBOCC results both show that there must also be enhanced conductivity in the mantle underlying the C1 conductor. Additional constrained inversions, not shown here, indicated that it was not possible to fit the data to the same level of misfit with a uniformly conducting mantle.

The first set of constrained inversions also provides some information on the Tintina Fault Zone. In these inversions the tear at the upper surface of the wedge extended through the Tintina Fault Zone (Fig. 11). The resulting models confine the resistive region within the fault zone to depths above this break, showing that it is possible to fit the MT data with the resistor constrained to depths of < 15 km. A second set of constrained inversions was performed to further investigate the Tintina Fault by establishing the lateral and depth extent of the resistor (Fig. 12). The seismic reflection response of the fault zone is described by Cook et al. (2004), Evenchick et al. (2005) and Snyder et al. (2005).

The constrained inversions for the Tintina Fault were performed using only the REBOCC approach. In the inversions the fault was

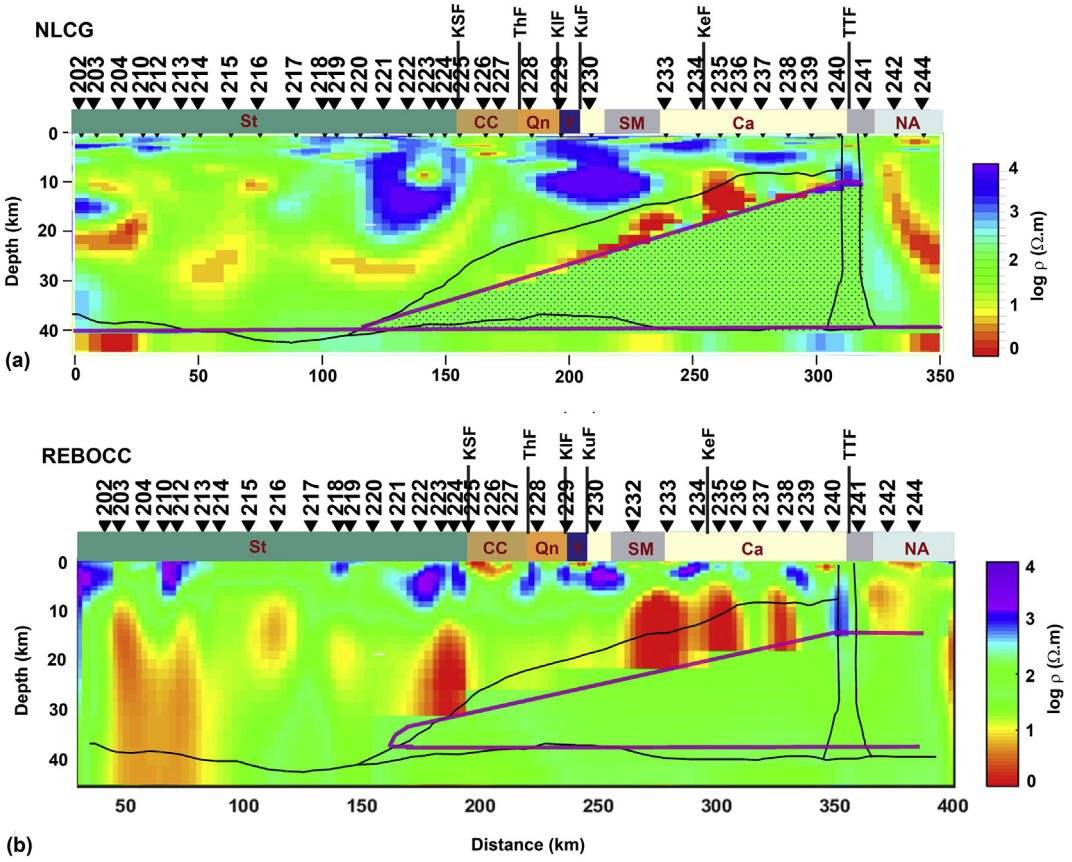

Fig. 11. (a) REBOCC and (b) NLCG resistivity model resulting from constrained inversion for Corridor 2a. The misfit for each model was either better or only marginally larger than the results for the corresponding unconstrained inversions. The black lines superimposed on the model show the seismically-defined location of the Moho, the Tintina Fault Zone, and the westward tapering wedge of reflective rocks (Cook et al., 2004). The purple lines show the approximate position of breaks in the smoothing in the inversion. In the NLCG inversion the resistivity of the seismic wedge has been fixed at 100 Ω·m. Note the slightly different colour scales for the two panels. (For interpretation of the references to colour in this figure legend, the reader is referred to the web version of this article.)

incorporated as a break in the smoothing with three different forms: i) a single vertical discontinuity located at the western margin of the seismically defined fault zone that extends from the surface to the base of the crust; ii) a single vertical discontinuity that penetrates from the surface into the lithospheric mantle to the depth of about 70 km; and iii) two vertical discontinuities that enclose a 10 km wide fault zone that extend to the upper mantle. The inversion approach was similar to that for the previous constrained inversions. The three final models are shown in Fig. 12 and yielded normalized rms misfits of 3.02, 3.05, and 3.09 respectively (compared with the unconstrained inversion result of 3.15). For the sites with responses most sensitive to the Tintina Fault Zone structure the misfit is similar for the first and second model but slightly worse for the third model (see Supplementary material).

In the constrained inversion models with only a single discontinuity, the resistor in the Tintina Fault Zone is constrained to depths of > 25 km (Fig. 12a and b). In the lower crust, the width of this feature is approximately 10 km, similar to the extent of the seismically defined fault zone. There is a weak extension of the resistive zone in the lower crust to depths below the Moho. This mantle response is not enhanced by the extension of the break in smoothing into the mantle lithosphere. In contrast to the first two inversion models, when there are two discontinuities included in the inversion, the resulting model includes a resistive fault zone extending from near the surface to the Moho, with a weak extension into the lithospheric mantle (Fig. 12c).

The constrained inversion results provide information on the aspects of the resistive zone that *must* be components of the true resistivity structure and features that *may* be component of the true structure. We can conclude that the Tintina Fault Zone definitely includes a resistive part at crustal depths. As determined in unconstrained inversions and constrained inversions with only a single vertical discontinuity, the width of this zone is approximately 10 km. The constrained inversions (Figs. 11 and 12) show that the resistive zone must have a vertical extent of at least 10 km. However, the MT method is unable to place any firm constraints on the exact depth range of the resistive zone. The MT data set can be fitted to a similar level by models in which the zone is in the upper crust and extends from 5 to 15 km (Fig. 11a and b), in which it is in the lower crust and extends from 20 to 35 km (Fig. 12a and b), and in which it extends from 5 to 35 km (Fig. 12c) (although the local misfit is slightly worse in the third case). Finally, none of the unconstrained constrained inversions include a strong extension of the resistive zone into the lithospheric mantle indicating that there is minimal support in the MT data for a mantle signature of the Tintina fault. This is not to say that the Tintina Fault does not penetrate into the mantle, as is expected for such a long fault, but rather that the MT data are insensitive to any resistivity signature of the structure at those depths.

5.4. Unconstrained and constrained inversions for Corridor 2B

The unconstrained 2-D inversion of the Corridor 2B MT data, obtained using the NLCG approach, is shown in Fig. 13a and the observed data and model response are compared in Fig. 14. The rms misfit of the model was 2.04. As shown in Fig. 14 the long-period response and the TE phase response are fitted the most poorly. Sites at the eastern end of the profile are all fitted quite well with rms misfit at sites sno266 to sno270 averaging1.60. In contrast, data fit is moderate for sites on the

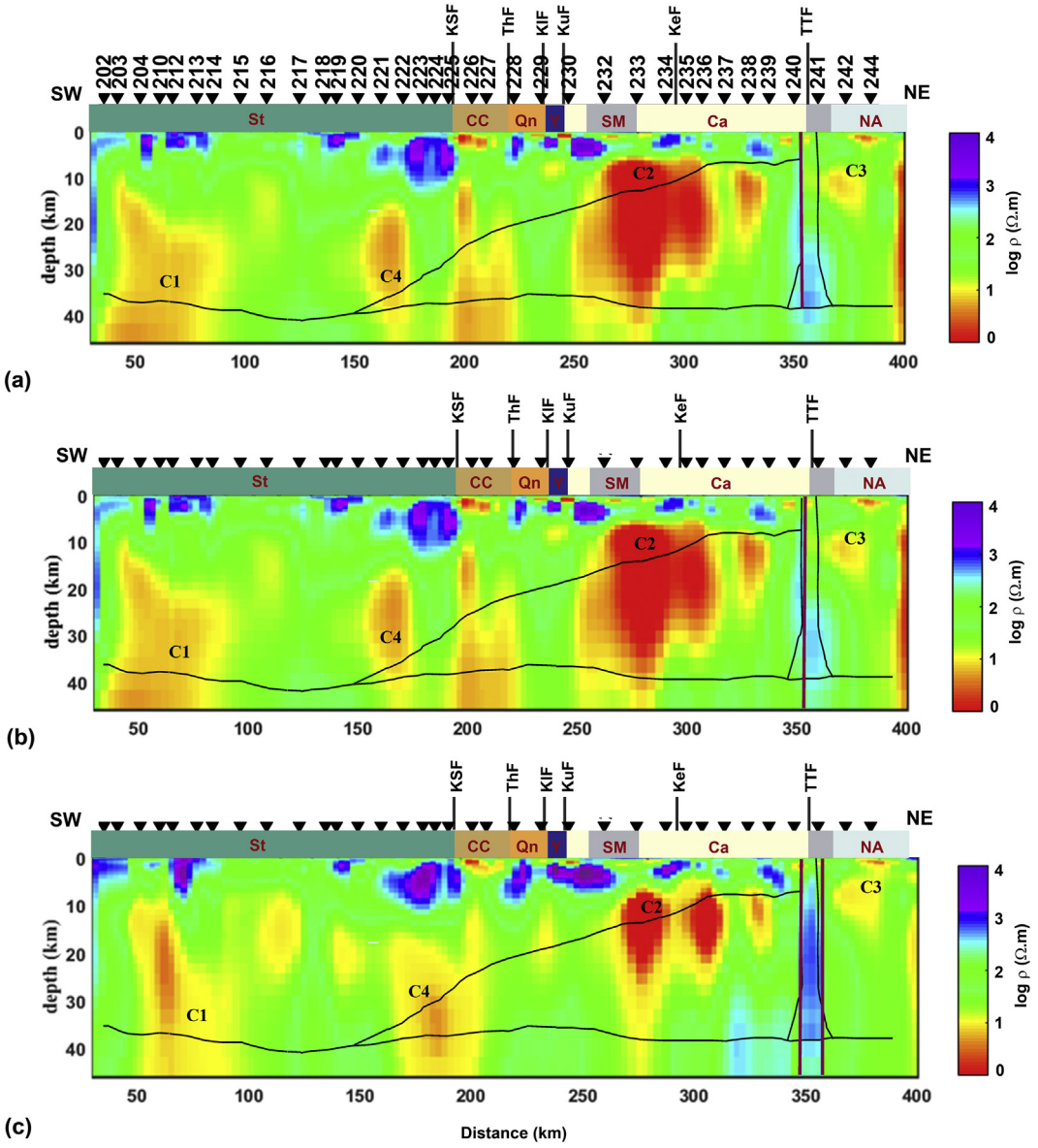

Fig. 12. REBOCC resistivity models resulting from inversion of Corridor 2A data with constraints on the geometry of the Tintina Fault Zone. The misfit for each model was superior to the result for the unconstrained inversion. Black lines superimposed on the model show the seismically-defined location of the Moho, Tintina Fault Zone, and the westward tapering wedge (Cook et al., 2004). Purple lines show the position of breaks in the smoothing applied in the inversion. Three geometries for the fault zone are considered. (a) Single vertical discontinuity from the surface to the base of the crust. (b) Single vertical discontinuity from the surface into the lithospheric mantle (70 km) (c) Two vertical discontinuities enclosing a 10 km wide zone and extending from the surface into the lithospheric mantle (70 km). (For interpretation of the references to colour in this figure legend, the reader is referred to the web version of this article.)

western end of the profile with rms misfit at sites sno239-sno245 averaging 2.10, and is poor in the middle of the profile with the rms misfit at sites sno246-sno261 averaging 2.25.

The near-surface region along Corridor 2B is characterized by a widespread conductive region (3–30 Ω·m) labelled C5 in Fig. 13 extending from sno244 in the west to sno270 in the east but discontinuous at the Muskwa Anticlinorium (between sno246-sno256). The conductor is defined by the data from numerous sites, and is a reliable component of the model. To the east of the Muskwa Anticlinorium it is approximately 3 km thick in the model, and to the west it is about 1 km thick, but the MT method provides poor resolution of the base of conductors. The areas of highest conductivity (< 5 Ω·m) occur at sno244-sno245 and between sno253 and sno267.

To the east of the Tintina Fault a conductive feature (C6 in Fig. 13) dips east, from 10 km depth into the lower crust. Although the data misfit is only moderate in this part of the profile, the existence of this feature is also established by its identification in data pseudosections: by east-dipping low apparent resistivity and high phase in the determinant phase (Fig. 5), and by east-dipping TE apparent resistivity and phase responses and TM phase responses (Fig. 14). This feature parallels strong reflections in both the seismic reflection (Cook et al., 2004; Evenchick et al., 2005) and wide-angle reflection results (Clowes et al., 2005).

The C6 conductor connects with a west-dipping conductor (C7) that projects to the surface near the western margin of the Muskwa Anticlinorium. The western margin of C7 and the break in the near-surface conductive layer at the Muskwa Anticlinorium are responsible for a resistive response in the determinant phase pseudosection (Fig. 5) and an increased strike response at crustal depth (Figs. 7 and 8). There is less confidence in the geometry of features of the resistivity model in this part of the profile because of increased rms misfit and because the profile between sites sno246 and sno258 is close to the strike. However,

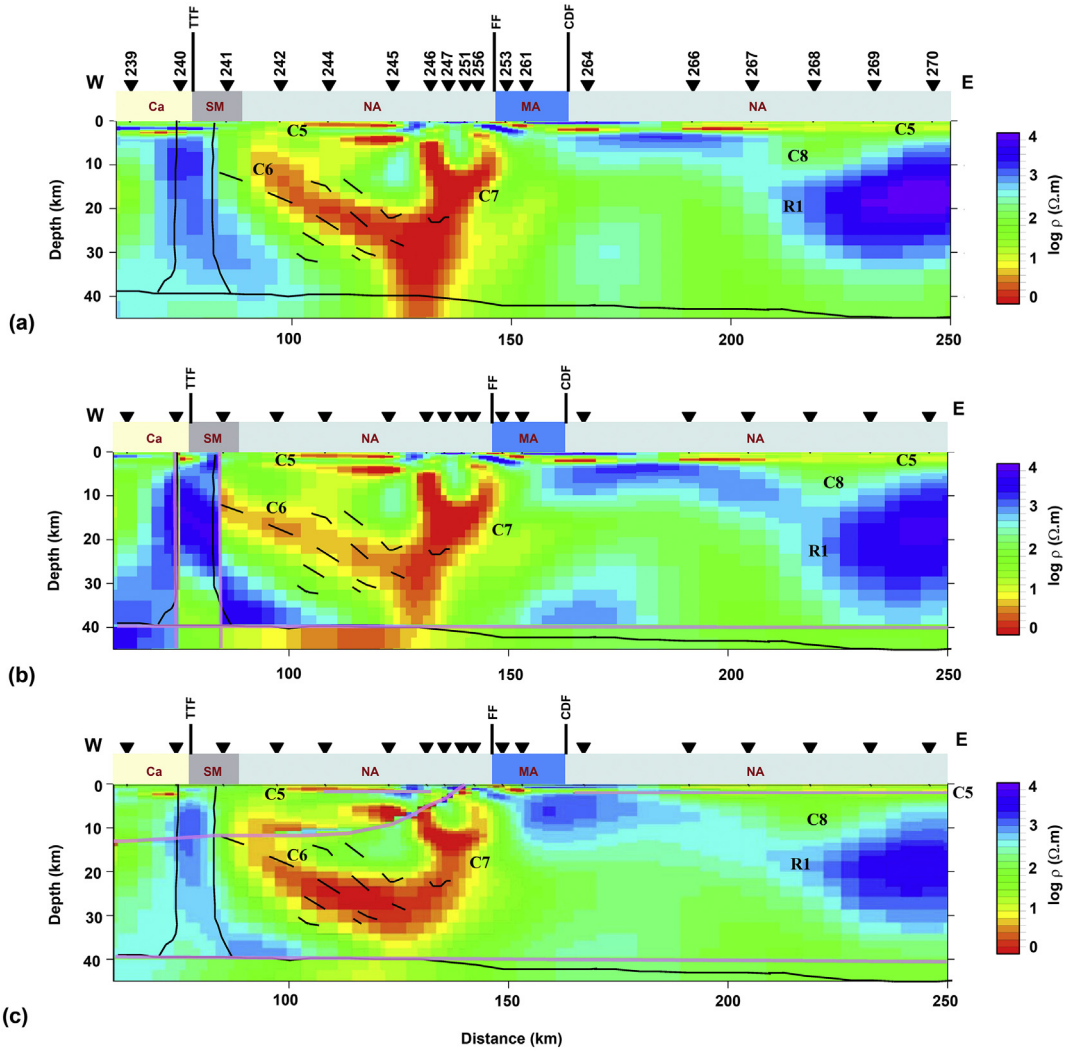

Fig. 13. Unconstrained and constrained NLCG 2D inversion models for Corridor 2b. The black lines superimposed on the model show the seismically-defined location of the Moho, the Tintina Fault Zone, and the prominent east dipping reflections east of the Tintina Fault (Cook et al., 2004). The purple lines show the approximate position of breaks in the smoothing applied in the inversion. (a) Unconstrained model; (b) model with regularization tears at the Moho and margins of the Tintina Fault Zone (enclosing a 10 km wide zone and extending from the surface to 70 km depth); (c) model with tears at the Moho, at an absolute depth of 2 km at the base of near-surface sedimentary rocks, and along the extension of the west tapering wedge east of the Tintina Fault (Cook et al., 2004). The normalized rms misfit of models (a), (b) and (c) is 2.04, 1.95, and 1.99 respectively. (For interpretation of the references to colour in this figure legend, the reader is referred to the web version of this article.)

it is of note that comparison of the seismic reflections results in Fig. 3 and the resistivity model in Fig. 12 shows that conductor C7 has a similar trend to two sets of west-dipping reflectors, one set extending from near vibration point 1600, and one set from the Muskwa Anticlinorium. Due to the N45°E azimuth of the Corridor 2B resistivity model, the two sets of reflections would be superimposed in the resistivity results. The geometry of C7 is investigated in constrained inversions below.

There are two additional conductors in the Corridor 2B resistivity model, beneath sites sno245 and sno246, with the base of the eastern one smeared into C7. Each of these other conductors is defined by the data from only one MT site so they are not considered to be robustly resolved features.

On the eastern end of the model the resistivity model includes a large wedge-shaped resistive feature (> 2000 Ω·m) in the crust labelled R1 in Fig. 13. In general, the MT method provides poor resolution of resistive zones located beneath conductive zones that possess higher integrated conductance (thickness-conductivity product). However, in this case the R1 feature is resolved by the data at multiple sites, sno267-sno270, which exhibit moderately good data fits, and it is supported by corresponding low phase and high apparent resistivity responses observed very clearly in the determinant and TE and TM pseudosections (Figs. 5 and 14). Although the existence of the feature is well established, its geometrical form and resistivity are poorly resolved. It is very possible that the feature extends farther to the west with its response in that area being masked by the increasing conductivity of the near-surface layer. The geometry of the base of the resistive feature is examined in constrained inversions below.

The resistive wedge is overlain by a westward thickening zone of moderate conductivity (30–100 Ω·m) labelled C8. Beneath sno268 this region has a thickness of approximately 10 km. The integrated conductance of the region (33 S beneath sno268), is comparable to that of the overlying near-surface conductive zone (23 S beneath sno268) suggesting that the geometry of C8 is reasonably well resolved, as the MT method provides good resolution of features with greater conductance than that present in overlying layers. However, as for the underlying resistive zone, it is possible that C8 extends farther west with its response in that area masked by increased conductivity in the near-surface zone.

In the first constrained inversion, the effect of breaks in the

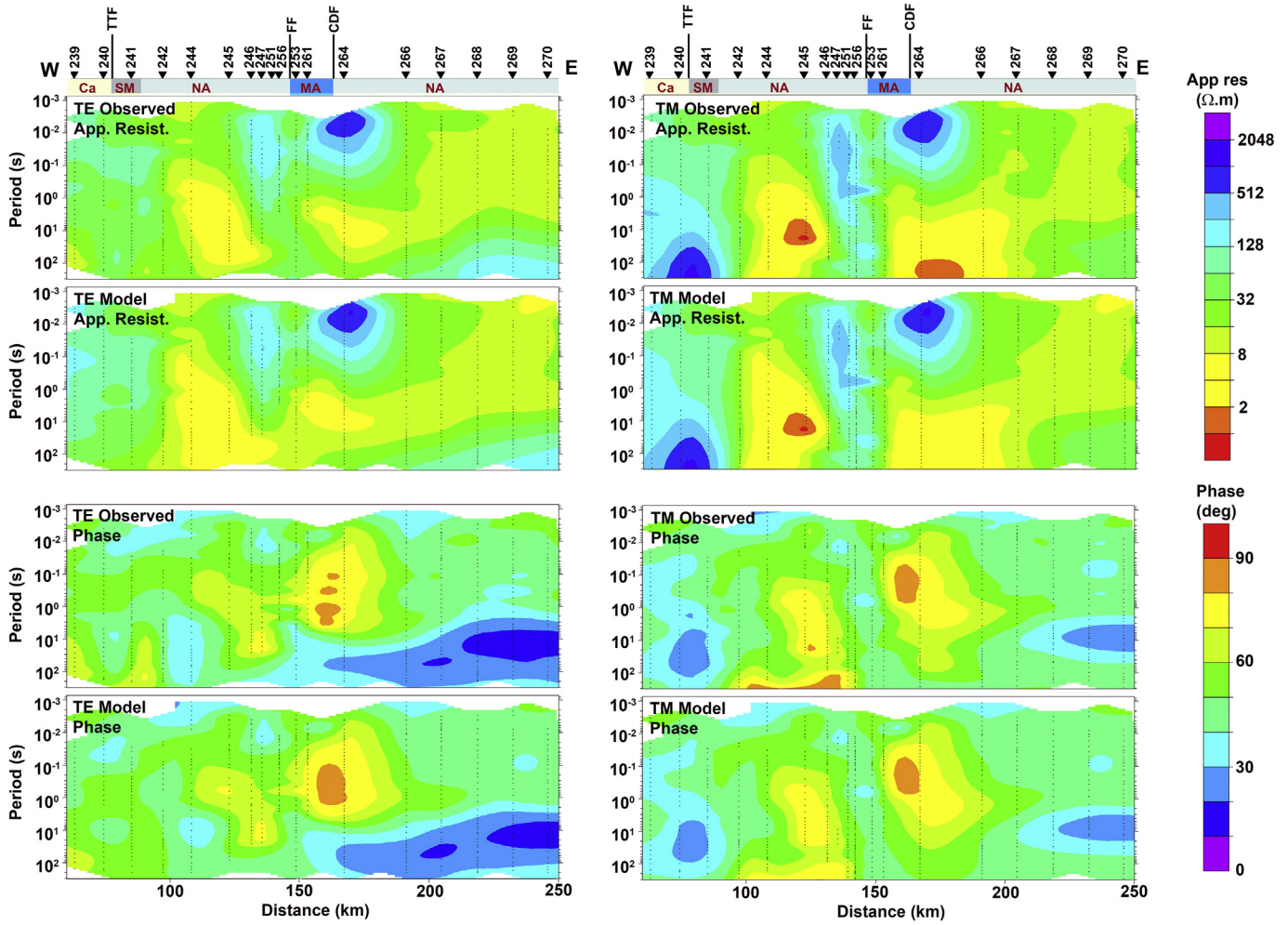

Fig. 14. Fit of the unconstrained NLCG inversion model to the observed data for the Corridor 2B inversion. The total normalized rms misfit for error floors applied (see details in the text) is 2.04. Left panels compare observed and model pseudosections of the apparent resistivity and phase response and right panels compare corresponding pseudosections for the TM response.

smoothing at the Moho and at the Tintina Fault Zone was examined (Fig. 13b). Comparisons of the data fit at representative sites for the unconstrained and constrained models are provided in the Supplementary material. The normalized rms misfit of the inversion model was 1.95 (compared with 2.04 for the unconstrained model). The inclusion of the tears at the Tintina Fault Zone show that the eastern end of conductor C2 may extend to a location adjacent to the fault zone. The inclusion of the tears at the Moho show that conductor C6 does not necessarily extend into the mantle but in this case the MT data do require an additional conductive zones on the upper mantle to the east of the Tintina Fault. The model also places the base of resistor R1 closer to the Moho than in the unconstrained model suggesting that R1 may extend to the Moho.

In the second constrained inversion tears were included at the Moho, the top of the westward tapering wedge (as defined by Cook et al., 2004), and the base of the surface sedimentary basin rocks west and east of the Muskwa anticlinorium (Fig. 13c). The normalized rms misfit of the inversion model was 1.99 (compared with 2.04 for the unconstrained model). The break at the base of the sedimentary basin rocks does not produce any significant change in the form of the underlying R1 and C8 features, but it does allow a more resistive zone to appear in the shallow crust beneath the Muskwa Anticlinorium. Additional constrained models were run with the tear at depths ranging from 1500 m to 3000 m. The results for the 2000 m depth yielded the most laterally uniform resistivity above and below the tear suggesting that this was the most reasonable depth.

The tear above the westward tapering wedge yields a model in which there are small conductive zones above the wedge surface but, in addition, conductors C6 and C7still occur within the wedge (Fig. 13c). The result indicates that C6 and C7 are not simply caused by smearing of shallow conductive zones. Shallow conductors above C6 and C7 are elongated features just above the wedge boundary. Additional constrained models were run in which model cells in the vicinity of C7 were constrained to a moderate resistivity value of 100 Ω·m. The results (not shown here) show that it is possible to fit the data without a continuous C7 conductor but in this case separated zones of enhanced conductivity still occur at the location of the top and basal parts of C7.

6. Resistivity structures in Ancestral North American rocks

6.1. Large-scale resistivity morphology

The crustal resistivity structure on Corridor 2 include two major lateral changes. The models show a major change between structures to the east and west of the Muskwa Anticlinorium and to the east and west of the Tintina Fault (Fig. 15). Between the Tintina Fault and the Muskwa Anticlinorium, the resistivity in the middle to lower crustal seismic wedge is dominated by a large synformal conductive zone. To the east of the Muskwa Anticlinorium the crust is relatively resistive and to the west of the Tintina Fault the wedge has uniform, moderate

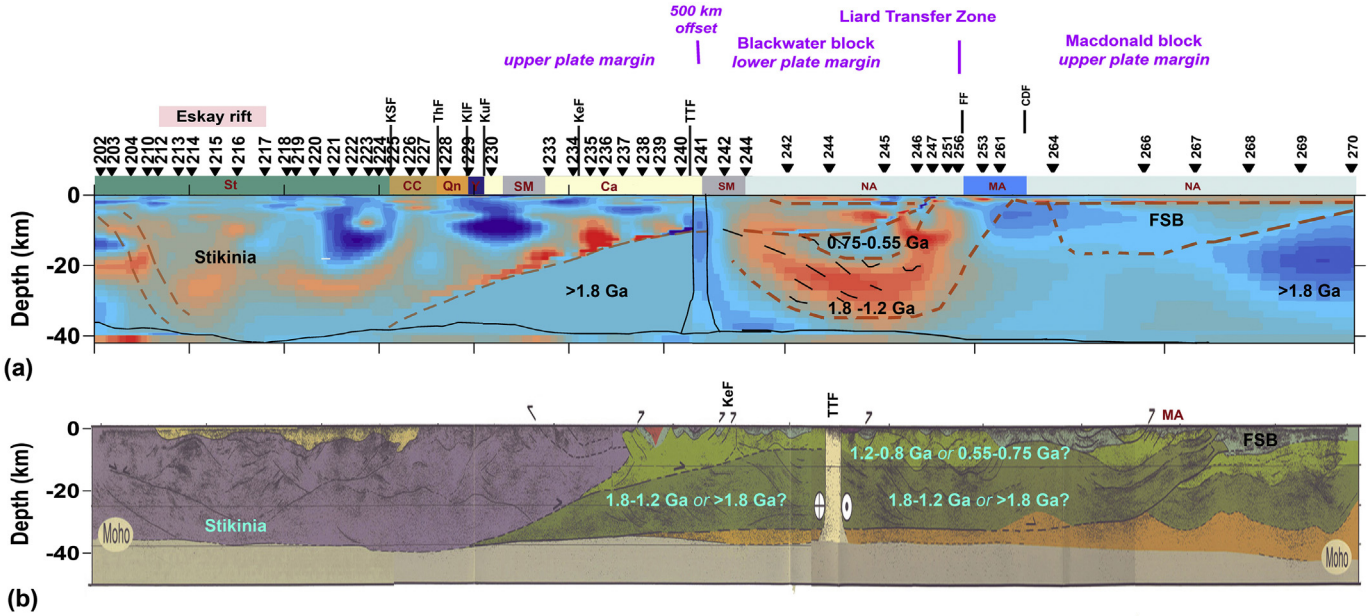

Fig. 15. Comparison of (a) integrated resistivity model for Corridor2 showing asymmetric rift segments and (b) interpreted seismic reflection results (modified from Lynn et al., 2005). The resistivity model is projected perpendicular to N45°W geoelectric strike whereas the seismic reflection results show true along-profile distance, resulting in relative offset of specific features. The interpretation of the age of the crust from the resistivity results is discussed in the text and is based on the interpretation of the synformal conductor east of the Tintina Fault as being associated with the Mesoproterozoic Muskwa Assemblage. The interpreted age of Proterozoic crust in the seismic models are from Cook et al. (2004) and Snyder et al. (2002, 2009) (first value) and Evenchick et al. (2005) (second value). Additional abbreviations: TeF = Teslin Fault. See Fig. 16 for resistivity colour scale.

resistivity. A similar change in resistivity character across the Tintina Fault is also observed on Corridor 3, although at that latitude the east dipping conductor is weaker than on Corridor 2 (Ledo et al., 2004).

In the N45°W projection, the eastern change in the resistivity structure coincides with both the Muskwa Anticlinorium and the Liard line (Figs. 1 and 15). The Liard line is a transfer zone in the asymmetric Neoproterozoic rifting, from upper plate rifting (see Fig. 2) in the Macdonald Block to the southeast to lower plate rifting in the Blackwater Block to the northwest (e.g., Hayward, 2015). The large-scale changes in the resistivity model on Corridor 2B can be interpreted in this context. As discussed below, the synformal conductor is interpreted as being associated with a deep sag basin. The changes at the Tintina Fault can also be explained in terms of rift geometry. Considering that motion on the Tintina Fault is of at least crustal extent (Abraham et al., 2001; Snyder et al., 2005), the 490 km offset on the fault will have juxtaposed the Blackwater Block, against a crustal block from farther to the southeast that underwent upper crustal rifting (Cecile et al., 1997; Lund, 2008), possibly the Peace River sub-block. Corridor 2a lies on an upper plate margin.

The geophysical data from Corridor 2B provide conflicting evidence on the presence of large-scale crustal changes such as those associated with the large offset on the Tintina Fault and juxtaposition of upper and lower plate margins at the Liard Transfer Zone. Seismic reflection data suggest the lower crustal seismic wedge contains a seismically continuous lower crustal layered sequence (Cook et al., 2004; Evenchick et al., 2005) and there is very consistent Moho depth across the Cordillera (Hyndman, 2017). These observations have led to interpretations that very similar rocks are present on either side of the Tintina Fault: Cook et al. (2004) interpret the wedge on both sides of the fault as consisting of Mesoproterozoic rocks whereas Evenchick et al. (2005) interpret it as consisting of mainly of older Proterozoic crystalline rocks of the Wopmay orogen.

In contrast to the larger-scale seismic reflection responses, there is geophysical and geochemical evidence for large-scale changes in the mid-lower crust and mantle lithosphere at the Tintina Fault and Liard transfer zone (Hayward, 2015). For example, the Tintina Fault Zone includes a near-vertical 15–20 km wide zone of weak and discontinuous reflectivity (Cook et al., 2004; Evenchick et al., 2005; Snyder et al., 2005) and there is evidence of local changes in Moho depth in the vicinity of the fault (Hayward, 2015). Near the Liard transfer zone (between vibrator points 1600 and 1800 in Fig. 3) the lower crustal reflectivity has greater transparency and less internal layering (Cook et al., 2004; Evenchick et al., 2005; Hayward, 2015). Seismic refraction results define a > 100 km wide zone of relatively low S-wave velocity between the Tintina Fault and Liard transfer zone extending to depths of 15 to 20 km (Fernández-Viejo et al., 2005). Modelling of gravity data by Hayward (2015) also defines a large-scale density contrast across the Liard line.

The MT results provide additional support for the interpretation of large-scale changes in crustal structure along Corridor 2B. The observation of significant differences in the crustal resistivity structure on either side of the Tintina Fault and Liard line (Fig. 15) suggests, although does not prove, that the rocks on either side of these features are different, a situation in accord with the juxtaposition of crust associated with different rift geometries. The correspondence of crustal-scale conductors C6 and C7 with seismic reflections within the Blackwater Block highlights the significance of these reflectors and defines a component of the seismic reflection response that can be used to support the interpretation of the large-scale changes.

6.2. Specific resistivity structures

6.2.1. Palaeozoic-Mesozoic rocks

Corridor 2B includes an extensive near-surface conductive zone of about 2 km thickness (Fig. 16). This feature can be reliably interpreted as being associated with Mesozoic and Palaeozoic sedimentary rocks of the Western Canadian Sedimentary Basin. These rocks are imaged clearly in the seismic reflection data (Cook et al., 2004; Evenchick et al., 2005). Thinning of the near-surface conductive layer between the Muskwa Anticlinorium and the Tuchodi Anticline is in accord with the seismic interpretation of Proterozoic rocks extending to the surface, or close to the surface, in this area (Cook et al., 2004; Evenchick et al.,

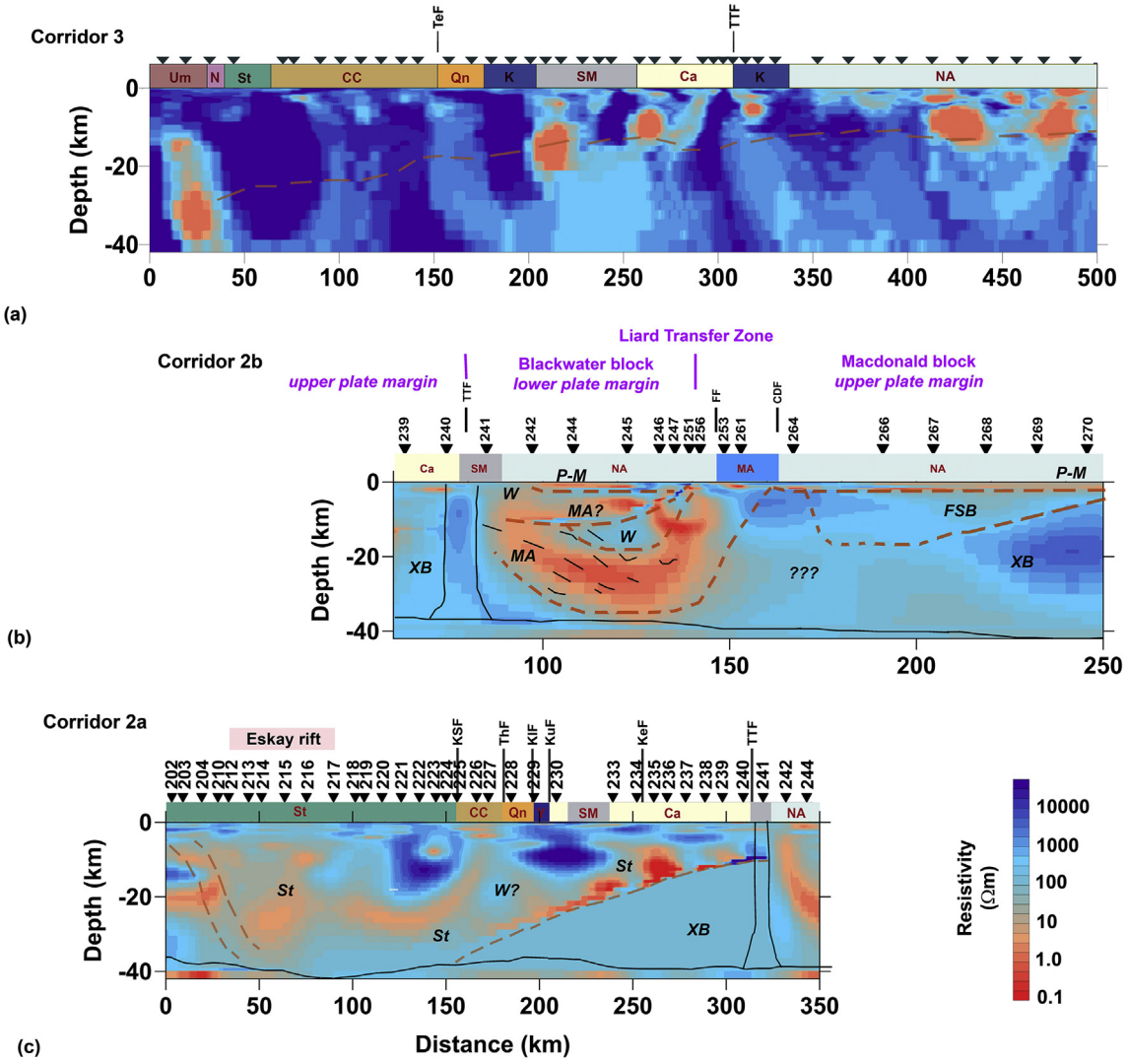

Fig. 16. Comparison of resistivity models. (a) Model for Corridor 3 (from Ledo et al., 2004). Dashed brown line defines the upper surface of westward tapering seismic wedge. Additional abbreviations: Um = Undivided metamorphic rocks, N = Nisling terrane. (b) Interpretation of crustal structure along LITHOPROBE Corridor 2B based on constrained inversion resistivity model. Purple text shows the location of different styles of asymmetric plate margins and dashed brown line shows interpretations discussed in the text. Abbreviations: XB = Crystalline basement, MA = Muskwa assemblage, FSB = Fort Simpson Basin, W = Windermere assemblage, P-M = Palaeozoic and Mesozoic rocks. (c) Interpretation of crustal structure along LITHOPROBE Corridor 2A based on constrained inversion resistivity models. All resistivity models are plotted using plotted using the colour scale in lower right. (For interpretation of the references to colour in this figure legend, the reader is referred to the web version of this article.)

2005).

6.2.2. Resistivity structures within the west-tapering wedge

Based on the geometry, and the consideration of potentially conductive rocks, it is most probable that the synformal conductor to the east of the Tintina Fault (crustal conductors C6 and C7 in Fig. 13) is associated with Muskwa Assemblage rocks. This interpretation is consistent with the interpretation of seismic reflection results by Cook et al. (2004) that the middle to lower crust in this region consists of Muskwa rocks (Fig. 3). The east-dip of conductor C6 parallels strong seismic reflections in these rocks and, although it is more poorly defined, conductor C7 also follows the trend of west dipping reflections (one set extending from near vibration point 1600, and one set extending from the Muskwa Anticlinorium).

There is strong evidence that the Muskwa Assemblage contains very conductive rocks. The Aida Formation includes a 60 m thick unit of carbonaceous mudstone 180 m above the base of the formation (Taylor and Stott, 1973). The Aida Formation rocks were intensely deformed during Cretaceous to Eocene orogenic activity forming the structures of the Muskwa Anticlinorium but still have relatively low metamorphic grade (Taylor and Stott, 1973; Cook et al., 2012). Globally, carbonaceous sedimentary rocks, such as those observed in the Aida Formation represent a major source of significant resistivity anomalies. For example, in Ontario a 400 m thick sequence of conductive black shales in Upper Ordovician formations obscures geoelectric imaging of much of the underlying crust (Mareschal et al., 1991) and in Europe the Alum shale has a major influence on the geoelectric response (e.g., Korja et al., 2008; Habibian et al., 2010). There are also reports of more intense localized mineralization in the Aida formation increasing the likelihood that these rocks are responsible for significant conductivity anomalies. Mineralization is reported in the Toro-Churchill Property ("TC" in Fig. 1; Reliance Geological Services Inc., 1996) and the Eagle Property ("EP" in Fig. 1) contains mineralized quartz-carbonate veins and alteration along fracture planes with development of graphite (British Columba Ministry of Energy and Mines and Responsible for Core Review, Minfile Record Summary, Minfile Number 094K 012).

Lower plate rift models include a thick sag basin underlain by highly deformed continental crust (e.g., Lister et al., 1986; Lund, 2008;

Hayward, 2015). The interpretation of the synformal conductive feature as being associated with pre-rift Muskwa sedimentary rocks is consistent with this model. In this interpretation it is most likely that the conductor consists of a series of deformed rotated blocks containing Muskwa rocks. The MT method has insufficient resolution to resolve such features but instead images the Muskwa rocks as a single conductor.

An alternative explanation of the synformal conductor is that it is associated with Paleoproterozoic crystalline rocks. As noted above, some conductive rocks are observed in the Wopmay orogen on Corridor 1. This alternative interpretation would follow Evenchick et al. (2005) who interpret the middle to lower crust in that area to consist of crystalline basement (Fig. 3). However, based on the coincidence of conductor C7 with seismic reflections that can be traced to surface Muskwa rocks we favour the alternative interpretation in terms of the conductor being associated with Muskwa rocks.

Absence of crustal conductors in the Ancestral North American wedge west of the Tintina Fault and east of the Liard line (Fig. 15) suggests the presence of different rocks in those locations. Candidates include Proterozoic crystalline basement rocks, as suggested by Evenchick et al. (2005), and Proterozoic sedimentary rocks of the Wernecke, Mackenzie Mountain, and Windermere supergroups. It is also possible that the lowermost crust contains a component of underplated material formed during the rifting process. MT results provide minimal discrimination between these possibilities. The MT results do resolve a more resistive wedge of rocks ($> 1000\ \Omega$·m) in the middle to lower crust at the east end of the Corridor. Given the location of this feature it is most reasonable to interpret it as consisting of crystalline Wopmay crust. The upper surface of the feature has a form similar to the geometry of Laurentian crust interpreted by Snyder et al. (2009) and its wedge shape is similar to geometries observed in Wopmay crust on Corridor 1 (Cook et al., 1999).

6.2.3. Fort Simpson Basin

East of the Muskwa Anticlinorium, the near-surface conductive zone is underlain by a thick zone of moderate conductivity (C8 in Fig. 13). Based on the clear spatial correlation of this feature with a region of low P- and S-wave seismic velocity defined in seismic refraction results (Clowes et al., 2005; Fernández-Viejo et al., 2005), and the trend of the Fort Simpson gravity high, the feature can be confidently interpreted as being associated with the Fort Simpson Basin (Fig. 16). MT results indicate that the basin has moderate resistivity and thickens to the west.

Background information on the Fort Simpson Basin comes from SNORCLE Corridor 1 to the northeast. The seismic reflection results defined three distinct zones in the basin (Cook et al., 1999). There is uncertainty over the exact origin of the rocks in the basin, but one possibility is that the zones correspond to the < 1.84 Ga to > 1.71 Ga Wernecke Supergroup, the 1.0–0.78 Ga Mackenzie Mountain Supergroup, and the < 0.78 Ga Windermere Supergroup. Alternatively, two or three of the zones could correspond to the Wernecke Supergroup (Cook et al., 1999). The Corridor 1 MT survey imaged relatively resistive ($> 400\ \Omega$·m) rocks (Wu et al., 2005). It is possible that the resistivity may have been increased by intrusive igneous rocks as enhanced magnetic responses over the basin have been explained by the presence of sills, flows, or dykes (e.g., Cook et al., 2005). Nevertheless, the MT results indicate that the Paleoproterozoic to Neoproterozoic rocks in the basin contain no prominent conductivity anomalies.

On Corridor 2 the Fort Simpson Basin hosts no major conductors but its resistivity ($\sim 100\ \Omega$·m) is less than on Corridor 1 ($> 450\ \Omega$·m). It is possible that the change is due to absence of intrusive rocks on the southern profile, and this interpretation is consistent with the strong Fort Simpson Magnetic High tracking past the eastern end of Corridor 2 (Lynn et al., 2005; Hayward, 2015). The MT results suggest that potential rocks in the basin, the Wernecke Supergroup, Mackenzie Mountain Supergroup, and the Windermere Supergroup have only moderate conductivity supporting the earlier interpretation of conductive Proterozoic crust as being due to the Muskwa Assemblage. Descriptions of outcropping Windermere Supergroup rocks in the northern Cordillera also provide no evidence for widespread graphitic rocks (Evenchick, 1988).

6.2.4. Middle crust in the Blackwater Block

The region above the conductive synform in the Blackwater Block contains rocks of moderate resistivity (Figs. 15, 16). If the conductor itself is associated with the Mesoproterozoic Muskwa Assemblage the more resistive overlying rocks represent moderately resistive younger units. In lower plate rift models, the thick sag basin is filled with syn-rift sediments, so it is most likely the material of moderate resistivity overlying the conductive synformal feature consists of Neoproterozoic Windermere rocks.

7. Resistivity structures in Cordilleran rocks

7.1. Large-scale resistivity morphology

Inversion models for Corridor 2A resolve a spatially complex upper crustal resistivity structure, a series of conductors above the westward tapering seismic wedge, and several conductor zones in the lower crust of Stikinia (Figs. 15, 16). There are some correlations between the resistivity variations at depths less than a few kilometres and the various accreted terranes, e.g., the Cache Creek terrane is relative conductive and the Slide Mountain terrane contains very conductive rocks. In general, the 10–15 km MT site spacing precludes closer association of resolved resistivity structures with specific geological features. It is also difficult to interpret the lower resolution resistivity images in terms of individual reflection packages (Cook et al., 2004; Evenchick et al., 2005; Calvert, 2016). Many of these packages have continuous reflection geometry over zones that are only 10 km wide and over only a few seconds of two-way travel time. If there are distinct resistivity structures in the individual reflective packages their response will be integrated with that of surrounding structures by the volume-averaging diffusion-based MT response.

The resistivity models derived for Corridor 2 show a number of similarities with the model for Corridor 3 and resistivity features for individual terranes and structures are compared below. For the resistivity models shown in Fig. 16, the overall crustal resistivity for Corridor 3 is higher than for Corridor 2. This result may be due in part due to the specific parameters used in the inversions, e.g., the resistivity of the starting model. It is also due to the presence of resistive crustal rocks at the southwestern end of Corridor 3. These rocks lie in the geomorphological Coast Belt and this belt was not crossed by Corridor 2.

7.2. Specific resistivity structures

7.2.1. Cache Creek terrane

All MT models for Corridor 2A, for both inversion approaches, include a shallow east-dipping or synformal conductor ($< 10\ \Omega$·m) extending to a ~ 3 km depth in the Cache Creek terrane. The conductor in the REBOCC inversion models, a synformal body between the King Salmon and Thibert Faults, exhibits strong spatial correlation with shallow seismic reflection (e.g., Calvert, 2016). The MT results for Corridor 3 also show a small, strong, shallow conductor ($< 30\ \Omega$·m) in the western part of the Cache Creek terrane and moderately conductive ($< 300\ \Omega$·m) east-dipping features (Ledo et al., 2004).

There are several possible sources of enhanced electrical conductivity in the Cache Creek terrane: (a) argillitic sedimentary rocks present in the Upper Triassic to early Jurassic accretionary prism and subduction related accretionary complexes (Ash, 1994), (b) sulphide mineralization in arc rocks (Nelson and Colpron, 2007), and (c) altered serpentinites within dismembered ophiolite assemblages (Ash, 1994). The second possibility is supported by occurrences of massive sulphide

mineralization in arc rocks of the terrane. To the southeast of where the Cache Creek terrane is crossed by Corridor 2, primitive Kutcho arc rocks host the Kutcho Creek Cu-rich massive sulphide deposit and there is potential for equivalent deposits to occur elsewhere in the terrane (Mihalynuk and Cordey, 1997; Nelson and Colpron, 2007).

The ultramafic rocks area more likely source of the enhanced conductivity. However, higher resolution MT studies would be required to confirm this interpretation. In the Cache Creek terrane in the Atlin area, closer to Corridor 3, extensive serpentinization of harzburgite and dunite rocks is observed and extensive carbonatization (CO_2 metasomatism) has occurred along fault zones forming listwanite. Alteration products also include sulphides (Ash and Arksey, 1989). Near the Dease Lake area on Corridor 2 (near sno223 and sno225), a number of small ultramafic bodies occur along the King Salmon Fault. These bodies consist of serpentinite that has also undergone listwanite alteration (Logan et al., 2011). The King Salmon Fault is interpreted to have a relative shallow eastward dip (Calvert, 2016) so the geometry of the observed conductor is consistent with it being associated with carbonatized serpentinite rocks located along the King Salmon Fault.

7.2.2. Slide Mountain terrane

The Slide Mountain terrane contains very conductive rocks. Although the data from the two sites in the terrane, sno232 and sno233, had to be edited extensively because of very high distortion and three-dimensionality, the remaining part of the data set define a strong shallow conductor (< 6 Ω·m) in the Slide Mountain terrane at 2–3 km depth. Its geometry is poorly resolved by the limited MT data. Results from MT Corridors 3 and 5 indicate the enhanced shallow conductivity in the terrane is localized to Corridor 2 and the Sylvester Allochthon location (Wennberg, 2003; Ledo et al., 2004).

The rocks of the Slide Mountain terrane are derived from a marginal ocean basin (Colpron et al., 2006; Nelson and Colpron, 2007; Colpron and Nelson, 2009). However, the conductor is more reasonably attributed to localized mineralization rather than the ocean basin rocks. There are numerous mines in the Cassiar area within 15 km of sno232. The rocks of the area have been extensively affected by Early Cretaceous carbonation alteration and mineralization (Sketchley et al., 1986; Sketchley and Sinclair, 1991). At the Erickson Mine ("EM" in Fig. 1) disseminated and fracture controlled elemental carbon is present in sufficient abundance to form carbon veins. The veins are composed of 50 to 90% carbon, up to several metres thick, and can be traced for at least 10 m along strike (Sketchley and Sinclair, 1991). Although a single vein of this size may not form a suitable target for MT imaging, a more extensive network of connected or partially connected veins would form a larger-scale conductor.

The mineralization in the Sylvester Allochthon required addition of an enormous volume of CO_2, which is best explained by a deep source rather than a local magmatic source (Anderson and Hodgson, 1989). However, the mineralization also likely required a local contribution to the ore fluids from the local argillitic rocks (Anderson and Hodgson, 1989). This ore deposit model would appear to be appropriate for generating fairly extensive conductive regions that may be detected using the MT imaging as was performed recently at Olympic Dam (Heinson et al., 2018).

7.2.3. Bowser Basin and Upper Hazelton Group

Sites sno202-sno216 are in the Bowser Basin (Fig. 1). The upper few kilometres of the resistivity models for this part of the profile contains no obvious resistivity structure associated with the basin. The model contains variable resistivity in the range 60 to > 1000 Ω·m, which is similar to values in the underlying Stikinia crust. The absence of a distinct resistivity signature is surprising, as the marine clastic sedimentary rocks making up the basin may be expected to have low to moderate resistivity. The rocks of the basin have reached an appropriate metamorphic grade to be conductive: studies have shown coal seams in the basin are metamorphosed to meta-anthracite grade (Evenchick et al., 2003). The absence of a distinctive basin-style resistivity signature may therefore be caused by the extensive deformation the basin has undergone, including 44% shortening (Evenchick, 1991; Evenchick et al., 1993, 2005).

The resistivity model provides a strong indication that the upper Hazelton Group, which is exposed in a regionally extensive distribution around the margins of the Bowser Basin (Fig. 1) is discontinuous beneath the basin. The Abou member of the upper Hazelton Group contains a 20–25 m thick organic-rich siliceous shale (Ricketts et al., 1992; Gagnon et al., 2012) that is expected to be highly conductive (e.g., Boerner et al., 1996) and easily detected by the MT method, even if significantly deformed. The absence of any highly conductive signature at MT sites over the basin suggests the absence of this unit beneath the Corridor 2 sites.

7.2.4. Stikinia

The uppermost crust of Stikinia and Quesnellia is relatively resistive, containing regions of moderate resistivity (30–300 Ω·m) with localized areas of higher resistivity (> 1000 Ω·m). Similar responses are observed on Corridor 5 (Wennberg, 2003) and Corridor 3 (Ledo et al., 2004). The moderate to high resistivity values beneath these terranes are consistent with their arc origin and composition of Devonian to Triassic mafic to felsic volcanic, clastic and carbonate rocks (Monger and Price, 2002).

In contrast to the upper crust, the deeper crust of Stikinia on Corridor 2 contains significant conductive zones and this part of the crust is more conductive than on Corridor 3 (Fig. 15). The westernmost conductive zone is either a continuous east-dipping feature extending from 10 km depth to the base of the crust (C1 in Figs. 9, 11, 12 and 15) or two separate conductors, at 10–15 km and near the base of the crust lying on an east dipping trend. Conductors with similar geometry are observed on Corridor 3 (Ledo et al., 2004) about 400 km to the north, and in Alaska (Stanley et al., 1990) 900 km to the northwest. At both of these locations the conductor also occurs inboard of the Denali Fault and outboard of, or beneath, the Stikine terrane. Large eastward dipping conductors identified elsewhere in the Cordillera e.g., in Vancouver Island (Kurtz et al., 1986, 1990) and the Cascade subduction zone in Washington and Oregon (Wannamaker et al., 1989; Meqbel et al., 2014; Bedrosian and Feucht, 2014) have been interpreted as being associated with subduction processes. Ledo et al. (2004) discuss possible causes of the conductor on Corridor 3 and conclude that it is due to metasedimentary rocks emplaced and metamorphosed during Paleocene Kula plate subduction.

Stikinia, unlike terranes to the northeast, is interpreted to extend in depth over the whole crust (Evenchick et al., 2005) so an alternative explanation of the conductor is that it records subduction events older than the Paleocene one. Marsden and Thorkelson (1992) suggest that the Stikinia terrane underwent concurrent plate subduction for a period of 35 Myr on both its east and west sides during the Jurassic. In this case conductor C1, and possibly the similar structures observed on Corridor 3 and in Alaska, can be interpreted as representing the result of Mesozoic subduction at ~170 Ma and earlier rather than the Cenozoic subduction at > 50 Ma.

Geochemical data provides evidence for extensive fertilization of the upper mantle beneath Stikinia indicating long-lived subduction beneath the terrane. Basalts in the Jurassic Iskut River Formation exhibit a strong subduction signature (Barresi et al., 2015). Intrusions hosting major mineral deposits in the Eskay region have calc-alkalic to mildly alkalic affinity that Nelson and Colpron (2007) indicate is consistent with melting of upper mantle that had been previously metasomatised during repeated Devonian to Triassic subduction events. This model requires that the resistivity signature of the subduction was preserved during the docking of Stikinia with the outboard Alexander–Wrangellia block and farther to the north with the Nisling terrane.

The resistivity model includes zones of enhanced conductivity in the

crust beneath the Eskay rift (Figs. 15, 16). The geometry of the conductive region is not accurately defined by the 2-D models, but in all models there is increased conductivity extending eastwards in the lower crust to the northeast of the east-dipping conductive zone (e.g., Fig. 9). All of the resistivity models for Corridor 2A also include a conductor at 10 km depth beneath sno216. This location is approximately midway between (and ~50 km from) the Red Chris ("RC" in Fig. 1) and Schaft Creek ("SC" in Fig. 1) porphyry copper deposits (Nelson and Colpron, 2007). In some models (e.g., Fig. 9a) this conductor is isolated, but in other models (e.g., Fig. 9b) it connects to the southwest to the lower crustal conductors. MT studies in other locations have shown extensive areas of conductive crust below major areas of mineralization, such as beneath the Olympic Dam area in Australia (Heinson et al., 2006, 2018) and beneath the Abitibi subprovince of the Superior craton (Boerner et al., 2000). The Stikinia conductor is more spatially confined than in the cited cases but it may also be associated with mineralizing events. The geochemistry of basalts in the Iskut River Formation indicates spatially variable interaction of the mantle magmas with the crust (Barresi et al., 2015).

Farther east in Stikinia, there is a conductor C4 defined by sites sno220-sno223 with its top at 20–25 km depth. The constrained modelling results shown in Fig. 11 suggest the top of the conductor lies at significantly shallower depth than the top of the seismic wedge. Its base is not well resolved, and the feature could extend to the wedge. There is no comparable feature observed on Corridor 3 (Ledo et al., 2004). The conductor is spatially correlated with zones of fairly strong, dominantly east-dipping, reflectivity in the seismic reflection results (at 6–8 s two-way travel time between SP 6900 and 7600), which suggests the presence of conductive metasedimentary rocks in the lower crust. Alternative explanations for the lower crustal conductor are that it represents a remnant of Jurassic subduction from the east side of Stikinia or that it was produced by interactions between the fertilized mantle and the crust during Jurassic magmatic events.

7.2.5. Conductive zones above seismic wedge

Inversion models for Corridor 2A and 2B resolve a series of conductors lying above the seismic wedge (e.g., Figs. 15, 16). These conductors occur beneath sites sno230-sno233, sno235-sno236 and sno242-sno245. The westernmost conductor occurs at a depth of 20–30 km and the easternmost conductor at a depth of about 10 km. A remarkably similar set of conductors lies just above the seismic wedge in the resistivity models for Corridor 3. The conductors tend to correlate with regions of low reflectivity, but this result may be coincidental in that there is low reflectivity in the zone just above the wedge (Cook et al., 2004). There is no obvious correlation of the conductors with seismic refraction velocities (Clowes et al., 2005; Fernández-Viejo et al., 2005) or with gravity or magnetic anomalies (Lynn et al., 2005).

The similarity of the conductors on Corridor 2A and 3 suggest a common geographically widespread source. Such a distribution requires a broad distribution of both appropriate source rocks and appropriate metamorphic and deformational conditions. Ledo et al. (2004) suggest that the conductors on Corridor 3 are related to the deformation associated with the thrusting of younger rocks over the Proterozoic crustal wedge and this model is also appropriate for the conductors on Corridor 2. Significant conductors elsewhere are observed over dipping tectonic boundaries. In the Trans-Hudson Orogen, the North American Central Plains (NACP) conductor and Thompson Belt (TOBE) conductors, are associated with Proterozoic rocks draped over the dipping margins of the Archean Sask craton (e.g., Jones and Craven, 1990; Jones et al., 1997; Jones et al., 2005a; Gowan et al., 2009). Jones et al. (1997) attribute the enhanced conductivity in northern parts of the NACP conductor to syngenetic, structurally-driven, migration of sulphides into fold hinges to form connected conducting networks. The sulphides are derived from sediments deposited in an arc environment. In the southern part of the NACP, the enhanced conductivity has been attributed to graphitic metapelites that were developed during east–west compression and metamorphism associated with strain heating (Jones et al., 2005a; Gowan et al., 2009).

The geometry of the conductors overlying the middle to lower crustal seismic wedge in the Cordillera suggests that they can be attributed to similar strain-related structural and metamorphic processes. In outcrops of Windermere Supergroup rocks to the north and south of Corridor 2 the rocks are considerably thickened by east-verging thrust faults and folds (Evenchick et al., 2005). Although it is not certain that these structures extend to the seismic wedge, the results suggest that suitable contractual conditions for enhancing conductors occurred near the wedge. Studies indicate that the Mesozoic syn-deformational metamorphism of Windermere Supergroup rocks yielded temperatures of at least 500 °C and pressures of 5–8 kbar (Evenchick, 1988). However, in the case of graphitic conductors, depending on the oxygen fugacity graphite should still be stable at these conditions (e.g., Selway, 2014).

The source rocks for the conductors above the seismic wedge to the west of the Tintina Fault, and possibly also to the east, are interpreted to be rocks from the Stikine terrane. This terrane contains conductive zones and rocks from the terrane are interpreted to possibly extend as far east as the Kechika Fault (Evenchick et al., 2005; Calvert, 2016). Source rocks may be euxinic metasediments or sheared serpentinites derived from alteration of ultramafic rocks.

It is unclear whether rocks of Stikine terrane extend farther east of the Kechika and Tintina Faults. Cook et al. (2004) interprets the zone just above the wedge on Corridor 2B as Meso- to Neoproterozoic rocks, whereas Evenchick et al. (2003) interpret the zone as comprising Neoproterozoic sedimentary rocks and possible crystalline basement. If the conductors in this region are not due to Stikine rocks then the most likely alternative is rocks of the Muskwa Assemblage that contain a probable source of enhanced conductivity in the Aida Formation.

7.2.6. Tintina Fault Zone

The constrained and unconstrained inversion models from the current study support earlier results on the resistivity structure of the Tintina Fault (Ledo et al., 2002a), and in addition also demonstrate that the MT method places only limited depth constraints on the resistive part of the fault zone. The results show that the Tintina Fault Zone includes a resistive zone with a width of around 10 km. The MT data show the shallowest the top of this resistive zone could be is around 5 km but they place minimal constraints on its actual depth range beyond showing that it must be at least 10 km in vertical extent.

Ledo et al. (2002a) provide an interpretation of the similar resistivity structure associated with the Tintina Fault. The resistive zone (feature D in Ledo et al., 2002a) is interpreted as being due the absence of a conducting zone at mid-crustal levels in the fault zone, and may be attributed to the absence of circulating meteoritic or metamorphic fluids at this depth, or to the physical conditions within the fault that did not permit the precipitation of graphite. The more conductive region in the upper 5 km of the seismically-defined fault zone (Feature A in Ledo et al., 2002a) correlates spatially with a flower structure interpreted from seismic reflection data (Snyder et al., 2005) and was interpreted by Ledo et al. (2002a) as being caused by conducting minerals or, alternatively, but less likely, by saline fluids in fractures. Conductors on either side of the fault at depths of 5 to 20 km (features B and C in Ledo et al., 2002a) occur on both Corridors 2 and 3. The similarity of the geometry of these conductors is remarkable given the 490 km offset on the fault. The geometry of the conductors provides a strong indication that they are associated with deformation or shear heating associated with the motion on the Tintina Fault rather than being due to the primary lithology.

It is useful to consider the cause of the limited resolution of the resistivity zone using the MT method. The electromagnetic response of a narrow resistive zone includes electric charge accumulation on the sides of the body causing an increase in the TM mode apparent resistivity response. Such an enhancement is observed in the Corridor 2 pseudosections at sites near the Tintina Fault (Figs. 9 and 13) at periods

of > 1 s. At periods for which MT signal penetration exceeds the depth to the top of the body the charge accumulation will be approximately independent of period. As the depth resolution of the MT method mainly comes from the period variation, the MT method will provide low resolution of the depth extent of the resistive zone.

8. Conclusions

The MT data from SNORCLE Corridor 2 have been reanalysed in this study using modern tensor decomposition approaches and applications of two independent of unconstrained and constrained 2-D MT inversions. Constrained inversions incorporated geophysical results, including the top of mid to lower crustal metasedimentary wedge, the Moho, and the Tintina fault in order to better evaluate the consistency of the resistivity models with seismic and other geophysical and geological results. The results of the new analyses have provided a new resistivity image for Corridor 2b and a higher resolution resistivity image for Corridor 2a (compare Figs. 4 and 15).

The new resistivity model for Corridor 2 exhibits many similarities with that for Corridor 3 to the north (Ledo et al., 2004). Some of these features become more evident with the use of constrained inversions. Similarities include a prominent east-dipping conductor adjacent to, or in, Stikinia, a series of conductors just above the wedge of Ancestral North American rocks, and east-dipping conductive features in the seismic wedge to the east of the Tintina Fault. There are also some differences between the resistivity models for the two Corridors, but these can be tied to differences in the tectonic structure along the profiles including the presence of Coast Belt rocks and the Selwyn basin on Corridor 3 and the Sylvester Allochthon and Fort Simpson Basin on Corridor 2.

The resistivity structure reveals large-scale structures in the mid to lower crust. To the west of the Tintina Fault the seismically-defined westward tapering wedge of Ancestral North American rocks has uniform moderate resistivity as was also observed on Corridor 3. Just east of the Tintina Fault, the wedge of Ancestral North American rocks contains a prominent east dipping conductor that parallels prominent seismic reflections extending from 10 km to 30 km depth. Similar, although not as prominent, structures are observed on Corridor 3. The MT observations provide for interpretation of the seismic reflections as primary lithological structures rather than late deformational features. The change in the resistivity character of the Ancestral North American wedge at the Tintina Fault and a second crustal-scale change at the Liard line can be explained in terms of the asymmetric rift geometry of the Laurentian margin in the Neoproterozoic (e.g., Hayward, 2015). The Liard transfer zone separates upper plate rifting from the east in the Macdonald Block with lower plate rifting to the west in the Blackwater Block and the ~490 km offset on the Tintina Fault juxtaposes the upper plate rifted margin in the Blackwater Block on the east side of the fault against a lower plate rifted margin on the west side.

The MT models define a large crustal-penetrating synformal conductor in the Blackwater Block. It is interpreted be associated with carbonaceous rocks of the Aida Formation of the Muskwa Assemblage with the current geometry of this feature representing the redistribution of this unit at the base of a deep sag basin. The basin fill is interpreted as less conductive syn-rift sedimentary rocks of the Windermere Supergroup. This interpretation is consistent with the interpretation of seismic reflection results by Cook et al. (2004) who interpret the lower crust in the area to be of Muskwa assemblage age rather than the interpretation by Evenchick et al. (2003) who interpret the crust to be > 1.8 Ga crystalline rocks (Fig. 3). To the east of Liard line the resistivity models define structures in the Macdonald Block including the moderately conductive Fort Simpson Basin and a wedge of more resistive lower crust.

In the Canadian Cordillera the upper crustal resistivity variations across the Intermontane Belt reflect the accretion of different terranes onto the Ancestral North American Basement. The 10–15 km spacing of the SNORCLE MT profiles means that a number of these terranes are imaged by only one or two MT sites limiting the imaging of the full spatial variation of resistivity within each terrane. The MT results provide some useful variation and show resistivity variations can be interpreted in terms of lithological variations and alteration processes. East-dipping conductors observed in Stikinia on both Corridors 2 and 3 are interpreted as being associated with ~170 Ma subduction beneath the west of Stikinia that also contributed to the significant metasomatism of the Stikinia lithospheric mantle. Adjacent zones of enhanced conductivity at lower to middle crustal depths are consistent with geochemical results that show mantle-derived magmas involved some crustal interactions. Relatively high conductivity in the Cache Creek terrane can be attributed to carbonaceous listwanite alteration of ultramafic bodies on the east-dipping King Salmon Fault. High conductivity in the Slide Mountain terrane in the Sylvester Allochthon is interpreted in terms of local carbonaceous alteration. The absence of shallow high conductivity beneath Corridor 2 where it crosses the Bowser Basin suggests the upper Hazleton Group is discontinuous beneath the basin.

The crustal resistivity models also include features related to deformational processes. A series of localized conductors above the Ancestral North American Basement wedge is attributed to the deformation and metamorphic processes associated with the Mesozoic thrust faulting. To the west of the Tintina Fault the source rocks for the conductors are likely from the Stikinia terrane and to the east they may be Muskwa Assemblage rocks. The constrained inversions performed in the current study confirm earlier results showing that the Tintina Fault Zone includes a 10 km wide resistive region. The top of the resistive zone is a depth exceeding 5 km and the zone must have a vertical extent of at least 10 km. The similarity of conductors flanking the fault zone at 5–20 km depth on corridors 2 and 3 suggests that the resistivity features are related to the fault, in a similar manner to the conductors located above the middle to lower crustal wedge, and not to the primary lithologies alone.

Future studies of the SNORCLE MT data base will focus on the application of 3-D inversion methods. As again shown by the new dimensionality and strike analyses in this study, the MT data do contain some 3-D components and it is expected that superior resistivity models may be obtained through the application of appropriate 3-D inversion. Based on measures of the two-dimensionality of the MT data set, such as the along profile consistency of geoelectric strikes and correlation with regional geological trends, the 2-D approaches uses in this study, particularly with seismic constrained applied, have given a reliable indication of the location and general form of crustal resistivity structure. However, the exact of geometry of a number of features is poorly defined, including some structures in the vicinity of Sylvester allochthon, the westward dipping conductor near the Liard line, and the structure of the Muskwa Anticlinorium. In addition, the resistivity of the mantle lithosphere is relatively poorly defined in the 2-D inversions because of the strong increase of the three-dimensionality of the data at longer periods.

The results of the LITHOPROBE MT studies point to the value of future surveys in the Cordillera for mineral exploration, mineral systems study and geomagnetic hazard evaluation (Boggs et al., 2018). The results show local resistivity variations in the upper crust of the Cordillera related to alteration and mineralization indicating that higher resolution MT studies or alternative electromagnetic surveys could contribute to delineating these processes in a mining camp scale. At a mineral-systems scale, it would be valuable to image the lithospheric mantle and lower crust to the west of the Ancestral North American basement over a larger area than covered by the LITHOPROBE transects. Further deep-penetrating MT studies of the Eskay trough would be of significant interest. The lithospheric-scale variations in resistivity defined in the Canadian Cordillera have implications for geomagnetic hazards including induction of geomagnetic induced currents (GICs) on powerlines and pipe-to-soil potentials on pipelines. Studies in the

northwestern United States using synoptic Earthscope MT recordings have shown the resistivity structure can exert a strong control on the form of GICs (Love et al., 2018) and have highlighted the need for comparable data sets farther north, into the Canadian Cordillera.

Acknowledgements

The present study was made possible by the earlier financial, administrative, and field support for the LITHOPROBE SNORCLE MT study. The contributions of B. Habibian to the project were supported through a research leave funded by the University of Tehran. A. Adetunji helped set up parts of the MT analysis software. We thank the two reviewers and editors for their contributions and particularly Reviewer 2 for a very thoughtful contribution.

Appendix A. Supplementary data

Supplementary data to this article can be found online at https://doi.org/10.1016/j.tecto.2019.05.012.

References

Abraham, A.C., Francis, D., Polve, M., 2001. Recent alkaline basalts as probes of the lithospheric mantle roots of the northern Canadian Cordillera. Chem. Geol. 175, 361–386. https://doi.org/10.1016/S0009-2541(00)00330-2.

Adetunji, A., Ferguson, I.J., Jones, A.G., 2014. Crustal and lithospheric scale structures of the Precambrian Superior-Grenville margin. Tectonophysics 614, 146–169. https://doi.org/10.1016/j.tecto.2013.12.008.

Anderson, P.G., Hodgson, C.J., 1989. The structure and geological development of the Erickson gold mine, Cassiar District, British Columbia, with implications for the origin of mother-lode-type gold deposits. Can. J. Earth Sci. 26, 2645–2660. https://doi.org/10.1139/e89-225.

Ash, C.H., 1994. Origin and Tectonic Setting of Ophiolitic Ultramafic and Related Rocks in the Atlin Area, British Columbia (NTS 104N). Bulletin 94. Province of British Columbia, Ministry of Energy, Mines and Petroleum Resources, Vancouver.

Ash, C.H., Arksey, R.L., 1989. The Atlin ultramafic allochthon: ophiolitic basement within the Cache Creek Terrane; tectonic and metallogenic significance (104N/12). In: Geological Fieldwork 1989. Province of British Columbia Ministry of Energy and Mines, Vancouver, pp. 1990-1.

Audet, P., Sole, C., Schaeffer, A.J., 2016. Control of lithospheric inheritance on neotectonic activity in northwestern Canada? Geology 44, 807–810. https://doi.org/10.1130/G38118.1.

Barresi, T., Nelson, J.L., Dostal, J., 2015. Geochemical constraints on magmatic and metallogenic processes: Iskut River Formation, volcanogenic massive sulfide-hosting basalts, NW British Columbia, Canada. Can. J. Earth Sci. 52, 1–20. https://doi.org/10.1139/cjes-2014-0034.

Becken, M., Burkhardt, H., 2004. An ellipticity criterion in magnetotelluric tensor analysis. Geophys. J. Int. 159, 69–82. https://doi.org/10.1111/j.1365-246X.2004.02376.x.

Bedrosian, P.A., Feucht, D.W., 2014. Structure and tectonics of the northwestern United States from EarthScope USArray magnetotelluric data. Earth Planet. Sci. Lett. 402, 275–289. https://doi.org/10.1016/j.epsl.2013.07.035.

Bibby, H.M., Caldwell, T.G., Brown, C., 2005. Determinable and non-determinable parameters of galvanic distortion in magnetotellurics. Geophys. J. Int. 163, 915–930. https://doi.org/10.1111/j.1365-246X.2005.02779.x.

Boerner, D.E., Kurtz, R.D., Craven, J.A., 1996. Electrical conductivity and Paleo-Proterozoic foredeeps. J. Geophys. Res. Solid Earth 101 (B6), 13775–13791. https://doi.org/10.1029/96JB00171.

Boerner, D.E., Kurtz, R.D., Craven, J.A., 2000. A summary of electromagnetic studies on the Abitibi-Grenville transect. Can. J. Earth Sci. 37, 427–437. https://doi.org/10.1139/e99-063.

Boggs, K.J., Aster, R.C., Audet, P., Brunet, G., Clowes, R.M., de Groot-Hedlin, C.D., Donovan, E., Eaton, D.W., Elliott, J., Freymueller, J.T., Hedlin, M.A.H., Hyndman, R.D., James, T.S., Kushner, P.J., Morell, K.D., Rowe, C.D., Schutt, D.L., Sideris, M.G., Ulmi, M., Vernon, F.L., West, N., 2018. EON-ROSE and the Canadian Cordillera Array–building bridges to span Earth System Science in Canada. Geosci. Can. 45, 97–109. https://doi.org/10.12789/geocanj.2018.45.136.

Booker, J.R., 2014. The magnetotelluric phase tensor: a critical review. Surv. Geophys. 35, 7–40. https://doi.org/10.1007/s10712-013-9234-2.

ten Brink, U.S., Miller, N.C., Andrews, B.D., Brothers, D.S., Haeussler, P.J., 2018. Deformation of the Pacific/North America plate boundary at Queen Charlotte Fault: the possible role of rheology. J. Geophys. Res. Solid Earth 123, 4223–4242. https://doi.org/10.1002/2017JB014770.

Caldwell, T.G., Bibby, H.M., Brown, C., 2004. The magnetotelluric phase tensor. Geophys. J. Int. 158, 457–469. https://doi.org/10.1111/j.1365-246X.2004.02281.x.

Calvert, A.J., 2016. Seismic interpretation of crustal-scale extension in the Intermontane Belt of the northern Canadian Cordillera. Geology 44, 447–450. https://doi.org/10.1130/G37767.1.

Cecile, M.P., Morrow, D.W., Williams, G.K., 1997. Early Paleozoic (Cambrian to Early Devonian) tectonic framework. Canadian Cordillera. Bull. Can. Petrol. Geol. 45, 54–74.

Chave, A.D., 2012. Estimation of the magnetotelluric response function. In: Chave, A.D., Jones, A.G. (Eds.), The Magnetotelluric Method: Theory and Practice. Cambridge University Press, Cambridge, pp. 165–218.

Chave, A.D., Jones, A.G., 2012. The Magnetotelluric Method: Theory and Practice. Cambridge University Press, Cambridge (ISBN 978-0521819275).

Clowes, R.M., 1993. LITHOPROBE Phase IV Proposal – Studies of the Evolution of a Continent. LITHOPROBE Secretariat, Vancouver.

Clowes, R.M., Hammer, P.T., Fernández-Viejo, G., Welford, J.K., 2005. Lithospheric structure in northwestern Canada from Lithoprobe seismic refraction and related studies: a synthesis. Can. J. Earth Sci. 42, 1277–1293. https://doi.org/10.1139/e04-069.

Colpron, M., Nelson, J.L., 2009. A Palaeozoic Northwest Passage: incursion of Caledonian, Baltican and Siberian terranes into eastern Panthalassa, and the early evolution of the North American Cordillera. Geol. Soc., London, Sp. Pub. 318, 273–307. https://doi.org/10.1144/SP318.10.

Colpron, M., Nelson, J.L., Murphy, D.C., 2006. A tectonostratigraphic framework for the pericratonic terranes of the northern Canadian Cordillera. In: Colpron, M., Nelson, J.L. (Eds.), Paleozoic Evolution and Metallogeny of Pericratonic Terranes at the Ancient Pacific Margin of North America, Canadian and Alaskan Cordillera. Special Paper 45, Geol. Assoc. Canada, St. Johns, pp. 1–23.

Coney, P.J., Jones, D.L., Monger, J.W., 1980. Cordilleran suspect terranes. Nature 288, 329–333. https://doi.org/10.1038/288329a0.

Cook, F.A., Erdmer, P., 2005. An 1800 km cross section of the lithosphere through the northwestern North American plate: lessons from 4.0 billion years of earth's history. Can. J. Earth Sci. 42, 1295–1311. https://doi.org/10.1139/e04-106.

Cook, F.A., van der Velden, A.J., Hall, K.W., Roberts, B.J., 1999. Frozen subduction in Canada's Northwest Territories: LITHOPROBE deep lithospheric reflection profiling of the western Canadian Shield. Tectonics 18, 1–24. https://doi.org/10.1029/1998TC900016.

Cook, F.A., Clowes, R.M., Snyder, D.B., van der Velden, A.J., Hall, K.W., Erdmer, P., Evenchick, C.A., 2004. Precambrian crust beneath the Mesozoic northern Canadian Cordillera discovered by Lithoprobe seismic reflection profiling. Tectonics 23, 1–28. https://doi.org/10.1029/2002TC001412.

Cook, F.A., Hall, K.W., Lynn, C.E., 2005. The edge of northwestern North America at ~1.8 Ga. Can. J. Earth Sci. 42, 983–997. https://doi.org/10.1139/e05-039.

Cook, F.A., Erdmer, P., van der Velden, A.J., 2012. The evolving Cordilleran lithosphere. In: Percival, J.A., Cook, F.A., Clowes, R.N. (Eds.), Tectonic Styles in Canada: The Lithoprobe Perspective, Geological Survey of Canada, Special Paper 49, Geol. Ass. Canada, St. Johns, pp. 1–39.

Courtier, A.M., Gaherty, J.B., Revenaugh, J., Bostock, M.G., Garnero, E.J., 2010. Seismic anisotropy associated with continental lithosphere accretion beneath the CANOE array, northwestern Canada. Geology 38, 887–890. https://doi.org/10.1130/G31120.1.

Duba, A., Heikamp, S., Meurer, W., Mover, G., Will, G., 1994. Evidence from borehole samples for the role of accessory minerals in lower-crustal conductivity. Nature 367, 59–61. https://doi.org/10.1038/367059a0.

Eaton, D.W., Adams, J., Asudeh, I., Atkinson, G.M., Bostock, M.G., Cassidy, J.F., Ferguson, I.J., Samson, S., Snyder, D.B., Tiampo, K.F., Unsworth, M.J., 2005. Geophysical arrays to investigate lithosphere and earthquake hazards in Canada. EOS 86 (169), 173. https://doi.org/10.1029/2005EO170001.

Evans, R.L., 2012. Conductivity of earth materials. In: Chave, A.D., Jones, A.G. (Eds.), The Magnetotelluric Method: Theory and Practice. Cambridge University Press, Cambridge, pp. 50–95.

Evenchick, C.A., 1988. Stratigraphy, Metamorphism, Structure and Their Tectonic Implications in the Sifton and Deserters Ranges, Cassiar and Northern Rocky Mountains, Northern British Columbia. Bulletin 376, Geological Survey of Canada, Ottawa. (90 pp).

Evenchick, C.A., 1991. Structural relationships of the Skeena fold belt west of the Bowser Basin, northwest British Columbia. Can. J. Earth Sci. 28, 973–983. https://doi.org/10.1139/e91-088.

Evenchick, C.A., Ferri, F., Mustard, P.S., McMechan, M., Osadetz, K.G., Stasiuk, L., Wilson, N.S.F., Enkin, R.J., Hadlari, T., McNicoll, V.J., 2003. Recent Results and Activities of the Integrated Petroleum Resource Potential and Geoscience Studies of the Bowser and Sustut Basins Project, British Columbia. Current Research 2003-A13. Geological Survey of Canada, Ottawa.

Evenchick, C.A., Gabrielse, H., Snyder, D., 2005. Crustal structure and lithology of the northern Canadian Cordillera: alternative interpretations of SNORCLE seismic reflection lines 2a and 2b. Can. J. Earth Sci. 42, 1149–1161. https://doi.org/10.1139/e05-009.

Ferguson, I.J., Craven, J.A., Kurtz, R.D., Boerner, D.E., Bailey, R.C., Wu, X., Orellana, M.R., Spratt, J., Wennberg, G., Norton, M., 2005. Geoelectric responses of Archean lithosphere in the western Superior Province, central Canada. Phys. Earth Planet. Int. 150, 123–143. https://doi.org/10.1016/j.pepi.2004.08.025.

Ferguson, I.J., Jones, A.G., Chave, A.D., 2012. Case studies and geological applications. In: Chave, A.D., Jones, A.G. (Eds.), The Magnetotelluric Method: Theory and Practice. Cambridge University Press, Cambridge, pp. 480–544.

Fernández-Viejo, G., Clowes, R.M., Welford, J.K., 2005. Constraints on the composition of the crust and uppermost mantle in northwestern Canada: Vp/Vs variations along Lithoprobe's SNorCLE transect. Can. J. Earth Sci. 42, 1205–1222. https://doi.org/10.1139/e05-028.

Gabrielse, H., Monger, J.W.H., Wheeler, J.O., Yorath, C.J., 1991. Part A. Morphogeological belts, tectonic assemblages, and terranes. In: Gabrielse, H., Yorath, C.J. (Eds.), Geology of the Cordilleran Orogen in Canada, Geology of Canada, No. 4. Geol. Surv. Canada, Ottawa, pp. 15–28.

Gabrielse, H., Murphy, D.C., Mortensen, J.K., 2006. Cretaceous and Cenozoic dextral orogen-parallel displacements, magmatism, and paleogeography, north-central Canadian Cordillera. In: Haggart, J.W., Enkin, R.J., Monger, J.W.H. (Eds.), Paleogeography of the North American Cordillera: Evidence for and against Large-Scale Displacements. Special Paper 46, Geol. Assoc. Canada, St. Johns, pp. 255–276.
Gagnon, J.F., Barresi, T., Waldron, J.W., Nelson, J.L., Poulton, T.P., Cordey, F., 2012. Stratigraphy of the upper Hazelton Group and the Jurassic evolution of the Stikine terrane, British Columbia. Can. J. Earth Sci. 49, 1027–1052. https://doi.org/10.1139/e2012-042.
Gowan, E.J., Ferguson, I.J., Jones, A.G., Craven, J.A., 2009. Geoelectric structure of the northeastern Williston basin and underlying Precambrian lithosphere. Can. J. Earth Sci. 46, 441–464. https://doi.org/10.1139/E09-028.
Groom, R.W., Bailey, R.C., 1989. Decomposition of magnetotelluric impedance tensors in the presence of local three-dimensional galvanic distortion. J. Geophys. Res. (Sold Earth) 94, 1913–1925. https://doi.org/10.1029/JB094iB02p01913.
Habibian, B.D., Brasse, H., Oskooi, B., Ernst, T., Sokolova, E., Varentsov, I., EMTESZ Working Group, 2010. The conductivity structure across the Trans-European Suture Zone from magnetotelluric and magnetovariational data modeling. Phys. Earth Planet. Int. 183, 377–386. https://doi.org/10.1016/j.pepi.2010.08.005.
Hamilton, M.P., Jones, A.G., Evans, R.L., Evans, S., Fourie, C.J.S., Garcia, X., Mountford, A., Spratt, J.E., SAMTEX MT Team, 2006. Electrical anisotropy of South African lithosphere compared with seismic anisotropy from shear-wave splitting analyses. Phys. Earth Planet. Int. 158, 226–239. https://doi.org/10.1016/j.pepi.2006.03.027.
Hansen, V.L., Goodge, J.W., Keep, M., Oliver, D.H., 1993. Asymmetric rift interpretation of the western North American margin. Geology 21, 1067–1070. https://doi.org/10.1130/0091-7613(1993)021<1067:ARIOTW>2.3.CO;2.
Hayward, N., 2015. Geophysical investigation and reconstruction of lithospheric structure and its control on geology, structure, and mineralization in the Cordillera of northern Canada and eastern Alaska. Tectonics 34, 2165–2189. https://doi.org/10.1002/2015TC003871.
Heinson, G.S., Direen, N.G., Gill, R.M., 2006. Magnetotelluric evidence for a deep-crustal mineralizing system beneath the Olympic Dam iron oxide copper-gold deposit, southern Australia. Geology 34, 573–576. https://doi.org/10.1130/G22222.1.
Heinson, G., Didana, Y., Soeffky, P., Thiel, S., Wise, T., 2018. The crustal geophysical signature of a world-class magmatic mineral system. Sci. Rep. 8, 10608. https://doi.org/10.1038/s41598-018-29016-2.
Hyndman, R.D., 2010. The consequences of Canadian Cordillera thermal regime in recent tectonics and elevation: a review. Can. J. Earth Sci. 47, 621–632. https://doi.org/10.1139/E10-016.
Hyndman, R.D., 2017. Lower-crustal flow and detachment in the North American Cordillera: a consequence of Cordillera-wide high temperatures. Geophys. J. Int. 209, 1779–1799. https://doi.org/10.1093/gji/ggx138.
Jones, A.G., 1983. On the equivalence of the “Niblett” and “Bostick” transformations in the magnetotelluric method. J. Geophys. 53, 72–73.
Jones, A.G., 1999. Imaging the continental upper mantle using electromagnetic methods. Lithos 48, 57–80. https://doi.org/10.1016/S0024-4937(99)00022-5.
Jones, A.G., 2012. Distortion of magnetotelluric data: its identification and removal. In: Chave, A.D., Jones, A.G. (Eds.), The Magnetotelluric Method: Theory and Practice. Cambridge University Press, Cambridge, pp. 219–302.
Jones, A.G., Craven, J.A., 1990. The North American Central Plains conductivity anomaly and its correlation with gravity, magnetic, seismic, and heat flow data in Saskatchewan, Canada. Phys. Earth Planet. Int. 60, 169–194. https://doi.org/10.1016/0031-9201(90)90260-5.
Jones, A.G., Ferguson, I.J., 2001. The electric Moho. Nature 409, 331–333. https://doi.org/10.1038/35053053.
Jones, A.G., Garcia, X., 2006. Electrical resistivity structure of the Yellowknife River Fault Zone and surrounding region. In: Anglin, C.D., Falck, H., Wright, D.F., Ambrose, E.J. (Eds.), Gold in the Yellowknife Greenstone Belt, Northwest Territories: Results of the EXTECH III Multidisciplinary Research Project, Spec. Publ. 3, Mineral Deposits Div., Geol. Assoc. Can., St. John's, pp. 126–141.
Jones, A.G., Gough, D.I., 1995. Electromagnetic images of crustal structures in southern and central Canadian Cordillera. Can. J. Earth Sci. 32, 1541–1563. https://doi.org/10.1139/e95-126.
Jones, A.G., Chave, A.D., Egbert, G., Auld, D., Bahr, K., 1989. A comparison of techniques for magnetotelluric response function estimation. J. Geophys. Res. Solid Earth 94, 14201–14213. https://doi.org/10.1029/JB094iB10p14201.
Jones, A.G., Katsube, J., Schwann, P., 1997. The longest conductivity anomaly in the world explained: sulphides in fold hinges causing very high electrical anisotropy. J. Geomagn. Geoelectr. 49, 1619–1629. https://doi.org/10.5636/jgg.49.1619.
Jones, A.G., Ledo, J., Ferguson, I.J., 2005a. Electromagnetic images of the Trans-Hudson orogen: the North American Central Plains anomaly revealed. Can. J. Earth Sci. 42, 457–478. https://doi.org/10.1139/e05-018.
Jones, A.G., Ledo, J., Ferguson, I.J., Grant, N., McNeice, G., Spratt, J., Farquharson, C., Roberts, B., Wennberg, G., Wolynec, L., Wu, X., 2005b. The electrical resistivity structure of Archean to Tertiary lithosphere along 3,200 km of SNORCLE profiles, northwestern Canada. Can. J. Earth Sci. 42, 1257–1275. https://doi.org/10.1139/e05-080.
Jones, A.G., Ledo, J., Ferguson, I.J., Craven, J.A., Unsworth, M.J., Chouteau, M., Spratt, J.E., 2014. The electrical resistivity of Canada's lithosphere and correlation with other parameters: contributions from Lithoprobe and other programmes. Can. J. Earth Sci. 51, 573–617. https://doi.org/10.1139/cjes-2013-0151.
Korja, T., Smirnov, M., Pedersen, L.B., Gharibi, M., 2008. Structure of the Central Scandinavian Caledonides and the underlying Precambrian basement, new constraints from magnetotellurics. Geophys. J. Int. 175, 55–69. https://doi.org/10.1111/j.1365-246X.2008.03913.x.
Kurtz, R.D., DeLaurier, J.M., Gupta, J.C., 1986. A magnetotelluric sounding across Vancouver Island detects the subducting Juan de Fuca Plate. Nature 325, 596–599. https://doi.org/10.1038/321596a0.
Kurtz, R.D., DeLaurier, J.M., Gupta, J.C., 1990. The electrical conductivity distribution beneath Vancouver Island: a region of active plate subduction. J. Geophys. Res. 95, 10,929–10,946. https://doi.org/10.1029/JB095iB07p10929.
Ledo, J., 2006. 2-D versus 3-D magnetotelluric data interpretation. Erratum. Surv. Geophys. 27, 111–148. https://doi.org/10.1007/s10712-005-1757-8.
Ledo, J., Jones, A.G., 2001. Regional electrical resistivity structure of the southern Canadian Cordillera and its physical interpretation. J. Geophys. Res. Solid Earth 106, 30755–30769. https://doi.org/10.1029/2001JB000358.
Ledo, J., Jones, A.G., 2005. Upper mantle temperature determined from combining mineral composition, electrical conductivity laboratory studies and magnetotelluric field observations: Application to the intermontane belt, Northern Canadian Cordillera. Earth Planet. Sci. Lett. 236, 258–268. https://doi.org/10.1016/j.epsl.2005.01.044.
Ledo, J., Jones, A.G., Ferguson, I.J., 2002a. Electromagnetic images of a strike-slip fault: the Tintina Fault - northern Canadian Cordillera. Geophys. Res. Lett. 29. https://doi.org/10.1029/2001GL013408.
Ledo, J., Queralt, P., Marti, A., Jones, A.G., 2002b. Two-dimensional interpretation of three dimensional magnetotelluric data: an example of limitations and resolution. Geophys. J. Int. 150, 127–139. https://doi.org/10.1046/j.1365-246X.2002.01705.x.
Ledo, J., Jones, A.G., Ferguson, I.J., Wolynec, L., 2004. Lithospheric structure of the Yukon, northern Canadian Cordillera obtained from magnetotelluric data. J. Geophys. Res. 109, B04410. https://doi.org/10.1029/2003JB002516.
Leonard, L.J., Mazzotti, S., Hyndman, R.D., 2008. Deformation rates estimated from earthquakes in the northern Cordillera of Canada and eastern Alaska. J. Geophys. Res. Solid Earth 113 (B8), B08406. https://doi.org/10.1029/2007JB005456.
Lister, G.S., Etheridge, M.A., Symonds, P.A., 1986. Detachment faulting and the evolution of passive continental margins. Geology 14, 246–250. https://doi.org/10.1130/0091-7613(1986)14<246:DFATEO>2.0.CO;2.
Logan, J.M., Moynihan, D.P., Diakow, L.J., 2011. Dease Lake Geoscience Project, Part I: Geology and Mineralization of the Dease Lake (NTS 104J/08) and East-Half of the Little Tuya River (NTS 104J/07E) Map Sheets, Northern British Columba. Geological Fieldwork 2011, Paper 2012-1. Province of Britsh Columbia, Geological Survey, Vancouver, pp. 23–44.
Love, J.J., Lucas, G.M., Kelbert, A., Bedrosian, P.A., 2018. Geoelectric hazard maps for the Pacific Northwest. Space Weather 16, 1114–1127. https://doi.org/10.1029/2018SW001844.
Lowe, C., 1999. Application of the magnetic method in mineral exploration: fundamentals and recent developments. In: Lowe, C., Thomas, M.D., Morris, W.A. (Eds.), Geophysics in Mineral Exploration: Fundamental and Case Histories. Short Course Notes 14. Geol. Ass, Canada, St. Johns, pp. 131–162.
Lund, K., 2008. Geometry of the Neoproterozoic and Paleozoic rift margin of western Laurentia: implications for mineral deposit settings. Geosphere 4, 429–444. https://doi.org/10.1130/GES00121.1.
Lynn, C.E., Cook, F.A., Hall, K.W., 2005. Tectonic significance of potential-field anomalies in western Canada: results from the Lithoprobe SNORCLE transect. Can. J. Earth Sci. 42, 1239–1255. https://doi.org/10.1139/e05-037.
Mareschal, M., Kurtz, R.D., Chouteau, M., Chakridi, R., 1991. A magnetotelluric survey on Manitoulin Island and Bruce Peninsula along GLIMPCE seismic line J: black shales mask the Grenville Front. Geophys. J. Int. 105, 173–183. https://doi.org/10.1111/j.1365-246X.1991.tb03453.x.
Marsden, H., Thorkelson, D.J., 1992. Geology of the Hazelton volcanic belt in British Columbia: implications for the Early to Middle Jurassic evolution of Stikinia. Tectonics 11, 1266–1287. https://doi.org/10.1029/92TC00276.
Martí, A., Queralt, P., Ledo, J., 2009. WALDIM: a code for the dimensionality analysis of magnetotelluric data using the rotational invariants of the magnetotelluric tensor. Comput. Geosci. 35, 2295–2303. https://doi.org/10.1016/j.cageo.2009.03.004.
Mazzotti, S., Leonard, L.J., Hyndman, R.D., Cassidy, J.F., 2008. Tectonics, dynamics, and seismic hazard, in the Canada-Alaska Cordillera. In: Freymueller, J.T., Haeussler, P.J., Wesson, R.L., Ekström, G. (Eds.), Active Tectonics and Seismic Potential of Alaska, Geophysical Monograph Series. 179. American Geophysical Union, Washington, pp. 297–319.
McLellan, M., Schaeffer, A.J., Audet, P., 2018. Structure and fabric of the crust and uppermost mantle in the northern Canadian Cordillera from Rayleigh-wave tomography. Tectonophys 724, 28–41. https://doi.org/10.1016/j.tecto.2018.01.011.
McNeice, G.W., Jones, A.G., 2001. Multisite, multifrequency tensor decomposition of magnetotelluric data. Geophysics 66, 158–173. https://doi.org/10.1190/1.1444891.
Meqbel, N.M., Egbert, G.D., Wannamaker, P.E., Kelbert, A., Schultz, A., 2014. Deep electrical resistivity structure of the northwestern US derived from 3-D inversion of USArray magnetotelluric data. Earth Planet. Sci. Lett. 402, 290–304. https://doi.org/10.1016/j.epsl.2013.12.026.
Miensopust, M.P., Jones, A.G., Muller, M.R., Garcia, X., Evans, R.L., 2011. Lithospheric structures and Precambrian terrane boundaries in northeastern Botswana revealed through magnetotelluric profiling as part of the Southern African Magnetotelluric Experiment. J. Geophys. Res. Solid Earth 116 (B2). https://doi.org/10.1029/2010JB007740.
Mihalynuk, M.G., Cordey, F., 1997. Potential for Kutcho Creek Volcanogenic Massive Sulphide Mineralization in the Northern Cache Creek Terrane: A Progress Report. Geological Fieldwork 1996, Province of British Columbia. ,. Geological Survey, Province of British Columbia, Vancouver, pp. 157–170 ,.
Mihalynuk, M.G., Nelson, J., Diakow, L.J., 1994. Cache Creek terrane entrapment: Oroclinal paradox within the Canadian Cordillera. Tectonics 13, 575–595. https://doi.org/10.1029/93TC03492.
Monger, J.W.H., 1989. Overview of Cordilleran geology. In: Ricketts, B.D. (Ed.), Western Canada Sedimentary Basin: A Case Study. Canadian Soc. Petr. Geol, Calgary, pp.

9–32.
Monger, J., Price, R., 2002. The Canadian Cordillera: geology and tectonic evolution. CSEG Recorder 27, 17–36.
Mortensen, J.K., Dusel-Bacon, C., Hunt, J., Gabites, J., 2006. Lead isotopic constraints on the metallogeny of middle and late Paleozoic syngenetic base metal occurrences in the Yukon-Tanana and Slide Mountain/Seventymile terranes and adjacent portions of the North American miogeocline. In: Colpron, M., Nelson, J.L. (Eds.), Paleozoic Evolution and Metallogeny of Pericratonic Terranes at the Ancient Pacific Margin of North America, Canadian and Alaskan Cordillera. Special Paper 45. Geol. Ass. Canada, St. Johns, pp. 261–279.
Nelson, J.L., Colpron, M., 2007. Tectonics and metallogeny of the British Columbia, Yukon and Alaskan Cordillera, 1.8 Ga to the present. In: Goodfellow, W.D. (Ed.), Mineral Deposits of Canada: A Synthesis of Major Deposit-Types, District Metallogeny, the Evolution of Geological Provinces, and Exploration Methods. Special Publication 5, Geol. Assoc. Canada, St. Johns, pp. 755–791.
Nelson, J.L., Colpron, M., Piercey, S.J., Dusel-Bacon, C., Murphy, D.C., Roots, C.F., 2006. Paleozoic tectonic and metallogenetic evolution of pericratonic terranes in Yukon, northern British Columbia and eastern Alaska. In: Colpron, M., Nelson, J.L. (Eds.), Paleozoic Evolution and Metallogeny of Pericratonic Terranes at the Ancient Pacific Margin of North America, Canadian and Alaskan Cordillera. Special Paper 45. Geol. Assoc. Canada, St. Johns, pp. 323–360.
Niblett, E.R., Sayn-Wittgenstein, C., 1960. Variation of electrical conductivity with depth by the magneto-telluric method. Geophysics 25, 998–1008. https://doi.org/10.1190/1.1438799.
Nieuwenhuis, G., Unsworth, M., Pana, D., Craven, J., Bertrand, E., 2014. Three-dimensional resistivity structure of Southern Alberta, Canada: implications for Precambrian tectonics. Geophys. J. Int. 197, 838–859. https://doi.org/10.1093/gji/ggu068.
Park, S.K., Mackie, R.J., 1997. Crustal structure at Nanga Parbat, northern Pakistan, from magnetotelluric soundings. Geophys. Res. Lett. 24, 2415–2418. https://doi.org/10.1029/97GL02147.
Parker, R.L., 1980. The inverse problem of electromagnetic induction: existence and construction of solutions based on incomplete data. J. Geophys. Res. Solid Earth 85, 4421–4428. https://doi.org/10.1029/JB085iB08p04421.
Péron-Pinvidic, G., Manatschal, G., Masini, E., Sutra, E., Flament, J.M., Haupert, I., Unternehr, P., 2015. Unravelling the along-strike variability of the Angola–Gabon rifted margin: a mapping approach. Geol. Soc. London Sp. Pub. 438, 49–76. https://doi.org/10.1144/SP438.1.
Reliance Geological Services Inc., 1996. Assessment Report on the Toro-Churchill Property - Liard Mining Division, British Columbia, Canada for Aries Resource Corp (Operator) and Action Minerals Inc.
Ricketts, B.D., Evenchick, C.A., Anderson, R.G., Murphy, D.C., 1992. Bowser basin, northern British Columbia: constraints on the timing of initial subsidence and Stikinia-North America terrane interactions. Geology 20, 1119–1122. https://doi.org/10.1130/0091-7613(1992)020<1119:BBNBCC>2.3.CO;2.
Rippe, D., Unsworth, M.J., Currie, C.A., 2013. Magnetotelluric constraints on the fluid content in the upper mantle beneath the southern Canadian Cordillera: implications for rheology. J. Geophys. Res. Solid Earth 118, 5601–5624. https://doi.org/10.1002/jgrb.50255.
Ritter, O., Hoffman-Rothe, A., Bedrosian, P., Weckmann, U., Haak, V., 2005. Electrical conductivity images of active and fossil fault zones. Geol. Soc. London Sp. Pub. 245, 165–186. https://doi.org/10.1144/GSL.SP.2005.245.01.08.
Rodi, W., Mackie, R.L., 2001. Nonlinear conjugate gradients algorithm for 2-D magnetotelluric inversions. Geophysics 66, 174–187. https://doi.org/10.1190/1.1444893.
Rodi, W., Mackie, R.L., 2012. The inverse problem. In: Chave, A.D., Jones, A.G. (Eds.), The Magnetotelluric Method: Theory and Practice. Cambridge University Press, Cambridge, pp. 347–420.
Selway, K., 2014. On the causes of electrical conductivity anomalies in tectonically stable lithosphere. Surv. Geophys. 35, 219–257. https://doi.org/10.1007/s10712-013-9235-1.
Siripunvaraporn, W., Egbert, G., 2000. An efficient data-subspace inversion method for 2-D magnetotelluric data. Geophysics 65, 791–803. https://doi.org/10.1190/1.1444778.
Sketchley, D.A., Sinclair, A.J., 1991. Carbonate alteration in basalt, Total Erickson gold mine, Cassiar, northern British Columbia, Canada. Econ. Geol. 86, 570–587. https://doi.org/10.2113/gsecongeo.86.3.570.
Sketchley, D.A., Sinclair, A.J., Godwin, C.I., 1986. Early Cretaceous gold–silver mineralization in the Sylvester allochthon, near Cassiar, north central British Columbia. Can. J. Earth Sci. 23, 1455–1458. https://doi.org/10.1139/e86-139.
Snyder, D.B., Clowes, R.M., Cook, F.A., Erdmer, P., Evenchick, C.A., Van der Velden, A.J., Hall, K.W., 2002. Proterozoic prism arrests suspect terranes: insights into the ancient Cordilleran margin from seismic reflection data. GSA Today 12, 4–9. https://doi.org/10.1130/1052-5173(2002)012<0004:ppasti>2.0.co;2.
Snyder, D.B., Roberts, B.J., Gordey, S.P., 2005. Contrasting seismic characteristics of three major faults in northwestern Canada. Can. J. Earth Sci. 42, 1223–1237. https://doi.org/10.1139/e05-027.
Snyder, D.B., Pilkington, M., Clowes, R.M., Cook, F.A., 2009. The underestimated Proterozoic component of the Canadian Cordillera accretionary margin. Geol. Soc. London Sp. Pub. 318, 257–271. https://doi.org/10.1144/SP318.9.
Soyer, W., Unsworth, M., 2006. Deep electrical structure of the northern Cascadia (British Columbia, Canada) subduction zone: implications for the distribution of fluids. Geology 34, 53–56. https://doi.org/10.1130/G21951.1.
Spratt, J.E., Skulski, T., Craven, J.A., Jones, A.G., Snyder, D.B., Kiyan, D., 2014. Magnetotelluric investigations of the lithosphere beneath the central Rae craton, mainland Nunavut, Canada. J. Geophys. Res. Solid Earth 119, 2415–2439. https://doi.org/10.1002/2013JB010221.
Stanley, W.D., Labson, V.F., Nokelberg, W.J., Csejtey Jr, B., 1990. Denali fault system and Alaska Range of Alaska: Evidence for underplated Mesozoic flysh from magnetotelluric surveys. Geol. Soc. Am. Bull. 102 (2), 160–173.
Taylor, G.C., Stott, D.F., 1973. Tuchodi Lakes map-area, British Columbia (94K). In: Geological Survey of Canada. Memoir 373 Department of Energy, Mines and Resources, Canada.
Thorkelson, D.J., Abbott, J.G., Mortensen, J.K., Creaser, R.A., Villeneuve, M.E., McNicoll, V.J., Layer, P.W., 2005. Early and middle Proterozoic evolution of Yukon, Canada. Can. J. Earth Sci. 42, 1045–1071. https://doi.org/10.1139/e04-075.
Vozoff, K., 1991. The magnetotelluric method. In: Nabighian, M.N. (Ed.), Electromagnetic Methods in Applied Geophysics. vol. 2. Soc. Exploration Geophysicists, Tulsa, pp. 641–711.
Wannamaker, P.E., Booker, J.R., Jones, A.G., Chave, A.D., Filloux, J.H., Waff, H.S., Law, L.K., 1989. Resistivity cross section through the Juan de Fuca subduction system and its tectonic implications. J. Geophys. Res. 94, 14,127–14,144. https://doi.org/10.1029/JB094iB10p14127.
Weaver, J.T., Agarwal, A.K., Lilley, F.E.M., 2000. Characterization of the magnetotelluric tensor in terms of its invariants. Geophys. J. Int. 141, 321–336. https://doi.org/10.1046/j.1365-246x.2000.00089.x.
Weidelt, P., Chave, A.D., 2012. The magnetotelluric response function. In: Chave, A.D., Jones, A.G. (Eds.), The Magnetotelluric Method: Theory and Practice. Cambridge University Press, Cambridge, pp. 123–164.
Wennberg, G., 2003. Magnetotelluric Response of the Northern Cordillera: Interpretation of the Lithospheric Structure of the SNORCLE Transect, Corridor 2, Line 2a and Connector Line. M.Sc. Thesis. Univ. Manitoba, Winnipeg.
Wolynec, L.L., 2000. LITHOPROBE Magnetotelluric Crustal Study of the Carcross Area, Yukon Territory. B.Sc. (Hons.) Thesis. Univ. Manitoba, Winnipeg.
Wu, X., Ferguson, I.J., Jones, A.G., 2005. Geoelectric structure of the Proterozoic Wopmay Orogen and adjacent terranes, Northwest Territories, Canada. Can. J. Earth Sci. 42, 955–981. https://doi.org/10.1139/e05-042.
Yang, X., 2011. Origin of high electrical conductivity in the lower continental crust: a review. Surv. Geophys. 32, 875–903. https://doi.org/10.1007/s10712-011-9145-z.
Yin, Y., Unsworth, M., Liddell, M., Pana, D., Craven, J.A., 2014. Electrical resistivity structure of the Great Slave Lake shear zone, northwest Canada: implications for tectonic history. Geophys. J. Int. 199, 178–199. https://doi.org/10.1093/gji/ggu251.
Zaporozan, T., Frederiksen, A.W., Bryksin, A., Darbyshire, F., 2018. Surface-wave images of western Canada: lithospheric variations across the Cordillera–craton boundary. Can. J. Earth Sci. 55, 887–896. https://doi.org/10.1139/cjes-2017-0277.